Neuron

Article

Deconstructing the neural circuit underlying social hierarchy in mice

Graphical abstract

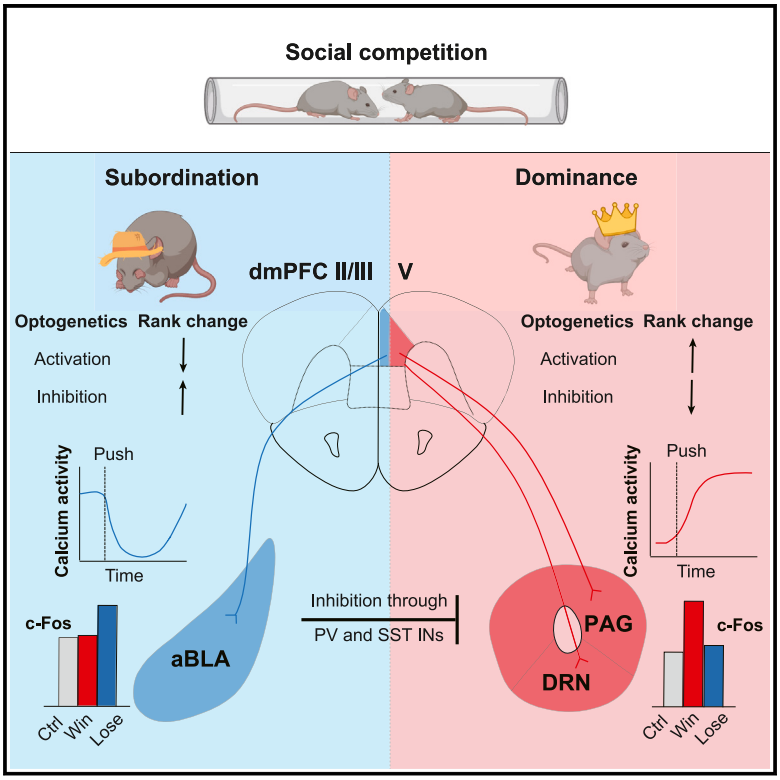

Highlights

- dmPFC-DRN and dmPFC-PAG pathways promote winning in social competition
- dmPFC-aBLA pathway promotes losing in social competition
- dmPFC layer 2/3 and layer 5 neurons oppositely regulate social competition
- Lose-related pathway inhibits win-related pathways

Authors

Qiuhong Xin, Diyang Zheng, Tingting Zhou, Jiayi Xu, Zheyi Ni, Hailan Hu

Correspondence

huhailan@zju.edu.cn

In brief

Xin et al. find that in the dorsomedial prefrontal cortex (dmPFC), layer 2/3 neurons projecting to the anterior basolateral amygdala promote losing, whereas layer 5 neurons projecting to the dorsal raphe nucleus and periaqueductal gray promote winning. Moreover, the lose-related pathway inhibits the win-related pathways through local GABAergic interneurons.

Xin et al., 2025, Neuron *113*, 1–16
February 5, 2025
https://doi.org/10.1016/j.neuron.2024.11.007

CellPress

Neuron

CellPress

Article

Deconstructing the neural circuit underlying social hierarchy in mice

Qiuhong Xin,[1,2] Diyang Zheng,[2] Tingting Zhou,[2] Jiayi Xu,[2] Zheyi Ni,[2] and Hailan Hu[1,2,3,*]

[1]Department of Neurobiology, Affiliated Mental Health Center & Hangzhou Seventh People's Hospital and School of Brain Science and Brain Medicine, Zhejiang University School of Medicine, Hangzhou 310058, China

[2]Nanhu Brain–Computer Interface Institute, MOE Frontier Science Center for Brain Science and Brain-Machine Integration, State Key Laboratory of Brain-Machine Intelligence, New Cornerstone Science Laboratory, Zhejiang University, Hangzhou 311121, China

[3]Lead contact

*Correspondence: huhailan@zju.edu.cn

https://doi.org/10.1016/j.neuron.2024.11.007

SUMMARY

Social competition determines hierarchical social status, which profoundly influences animals' behavior and health. The dorsomedial prefrontal cortex (dmPFC) plays a fundamental role in regulating social competitions, but it was unclear how the dmPFC orchestrates win- and lose-related behaviors through its downstream neural circuits. Here, through whole-brain c-Fos mapping, fiber photometry, and optogenetics- or chemogenetics-based manipulations, we identified anatomically segregated win- and lose-related neural pathways downstream of the dmPFC in mice. Specifically, layer 5 neurons projecting to the dorsal raphe nucleus (DRN) and periaqueductal gray (PAG) promote social competition, whereas layer 2/3 neurons projecting to the anterior basolateral amygdala (aBLA) suppress competition. These two neuronal populations show opposite changes in activity during effortful pushes in competition. *In vivo* and *in vitro* electrophysiology recordings revealed inhibition from the lose-related pathway to the win-related pathway. Such antagonistic interplay may represent a central principle in how the mPFC orchestrates complex behaviors through top-down control.

INTRODUCTION

Dominance-associated personality traits such as perseverance or motivational drive require higher cortical brain function.[1–4] The prefrontal cortex (PFC) has been shown to encode dominance status and competitive success in humans,[5,6] primates,[7] and rodents.[8–10] Manipulation of synaptic strength or neural activity in the dorsomedial prefrontal cortex (dmPFC, including the anterior cingulate cortex [ACC] and the prelimbic [PL] part of the PFC) neurons bidirectionally regulates the competitive outcomes and dominance status in the tube test,[8,11] reward competition,[9] and food foraging competition.[10] Collectively, these studies point toward the dmPFC as an evolutionally conserved central regulator of the dominance hierarchy.[12–16] While the upstream thalamic inputs to the dmPFC in social competition have been studied,[11,17,18] we still lack a brain-wide perspective of how the dmPFC coordinates downstream outputs to orchestrate complex dominance-related behaviors.

As an associative executive center,[19] the mPFC receives and integrates inputs from multiple sensory modalities and broadly projects to diverse regions throughout the brain, including the cortex, subcortex, and brainstem.[20–22] Through these projections, the mPFC exerts top-down control over a variety of behaviors,[23,24] including emotion regulation,[25] decision-making,[26,27] reward seeking,[28,29] effortful behavior,[30] motivation,[31] and cognitive flexibility.[32] In particular, a series of elegant studies have established the role of mPFC projections in regulating various social behaviors,[4,33] such as social approach avoidance (mPFC-basolateral amygdala [BLA]),[34] social learning (mPFC/ACC-BLA[35–37]; mPFC-lateral/ventrolateral periaqueductal gray [l/vlPAG][38]), reward competition (mPFC-lateral hypothalamus [LH]),[9] social preference (mPFC-nucleus accumbens [NAc]),[39] social defeat (mPFC-PAG),[17] and social competition (mPFC-NAc and mPFC-ventral tegmental area [VTA]).[40] Typically, these projection neurons in the mPFC display laminar organizations and are broadly distributed across layer 2 to layer 6.[22] Among them, a majority of BLA-projecting neurons tend to be found in layer 2/3, and NAc-projecting neurons are mostly localized in layer 2/3 and layer 5a,[39,41] with little overlap to each other.[39,42,43] Other subcortical regions, including the PAG, DRN, LH, and VTA, mainly received input from layer 5.[21,39,41] Although the mPFC downstream circuits involved in social dominance modulation are just beginning to be identified,[40] it remains to be explored how these different circuits engage in social competition and how the mPFC broadcasts dominance-related sensorimotor information into behavioral decisions via its output pathways.

In this work, in order to delineate the pathways downstream of the dmPFC in controlling social competition, we systematically screened the c-Fos immunoreactivity patterns in dmPFC downstream brain regions after social competition and focused on

Please cite this article in press as: Xin et al., Deconstructing the neural circuit underlying social hierarchy in mice, Neuron (2024), https://doi.org/10.1016/j.neuron.2024.11.007

brain areas that show differential c-Fos expression in the dominant and subordinate mice. Using pathway-specific optogenetics, we characterized the functional role of these mPFC downstream projections and identified several win- and lose-related pathways. Retrograde tracing and pathway-specific fiber photometry experiments revealed that win- and lose-related projection neurons are anatomically segregated and show opposing dynamic activity changes when mice engage in effortful pushes in the tube test competition. Notably, there is an inhibition from the lose-related pathway to the win-related pathway. Together, these results reveal a simple logic in how the dmPFC regulates competitive behaviors via its top-down control over different subcortical pathways.

RESULTS

Identification of win- or lose-activated brain regions downstream of the dmPFC

Using adeno-associated virus (AAV)-based strategy to label neurons with EGFP and axon terminals with synaptophysin-fused mRuby, we first mapped the brain-wide projections of the dmPFC (Figure S1A). We confirmed that the dmPFC broadly projects to diverse brain regions, among which the dmPFC axonal terminals are particularly abundant in several regions such as the BLA, caudate putamen (CPu), NAc, and mediodorsal thalamus (MDT) (Figure S1B). To determine the downstream regions of the dmPFC involved in social competition, we compared c-Fos immunoreactivity patterns throughout the brain, following tube tests in winner vs. loser mice, with mice passing through the tube without social confrontations serving as controls (Figure 1A). Ten brain regions were analyzed including the dmPFC, the ventral mPFC (vmPFC), and eight major subcortical downstream targets of the dmPFC. Significant differences in c-Fos expression were identified in five brain regions (Figure 1B). First, consistent with our previous report,[8] winner mice showed increased c-Fos expression in the dmPFC ($p = 0.02$, Friedman test with Dunn's multiple comparisons test; Figures 1B and 1C). In addition, a similar increase of c-Fos in winner mice was found in three subcortical areas downstream of the dmPFC: the MDT ($p = 0.02$), the dorsal raphe nucleus (DRN) ($p = 0.03$), and the PAG ($p = 0.003$) (Figures 1B and 1C). In contrast, c-Fos expression was increased in the loser but not winner mice in one brain region, the anterior BLA (aBLA) ($p = 0.02$; Figures 1B and 1C).

Altered dominance rank by inhibition of different dmPFC downstream circuits

To determine the functional role of different dmPFC projections in regulating social dominance, we next tried to inhibit these pathways by using AAV to bilaterally express eNpHR3.0 (an enhanced variant of the inhibitory halorhodopsin)[44] in the dmPFC and by implanting optic fibers above the various downstream areas (Figures 2 and S2; see STAR Methods and Figure S3). This allowed specific optogenetic inhibition of distinct dmPFC output terminals, respectively. After ranks were stable for at least 4 consecutive days, one of the four cagemate mice was photoinhibited immediately before it entered the tube to confront its opponent (Figure 2A; see STAR Methods). We systematically tested six pathways. Among them, inhibition of the dmPFC-MDT (Figures 2B–2D), dmPFC-dorsalmedial caudate putamen (dmCPu) (Figures S2A–S2C), and dmPFC-NAc (Figures S2D–S2F) pathways did not affect the tube test rank, while inhibition of the dmPFC-DRN (Figures 2E–2H) or dmPFC-PAG (Figures 2I–2L) yielded more retreats ($p < 0.0001$, U = 15 for dmPFC-DRN; $p < 0.0001$, U = 0 for dmPFC-PAG; Mann-Whitney U test; Figures 2H and 2L) and reduced tube test ranks (day 0, $p = 0.02$ for dmPFC-DRN and $p = 0.003$ for dmPFC-PAG, two-way repeated-measures ANOVA; Bonferroni multiple comparisons post hoc tests; Figures 2G and 2K). In contrast, photoinhibition of the dmPFC-aBLA (Figures 2M–2P) projection decreased retreats ($p = 0.0001$, U = 43.5, Mann-Whitney U test; Figure 2P) and increased dominance rank in 8 out of 11 mice tested in the tube tests (day 0, $p < 0.0001$, two-way repeated-measures ANOVA; Bonferroni multiple comparisons post hoc tests, Figure 2O).

Altered dominance rank by activation of different dmPFC downstream circuits

We next examined the consequence of activation of the dmPFC-DRN, dmPFC-PAG, and dmPFC-aBLA pathways (Figure 3) by injecting AAV virus encoding channel rhodopsin (ChR2) into the right dmPFC and by implanting optic fibers above the DRN, PAG, or aBLA (Figures 3A, 3E, and 3I; see STAR Methods and Figure S3). Consistent with the inhibition result, photostimulation of dmPFC-DRN or dmPFC-PAG promoted pushes and induced rank elevation in the tube test (day 0, $p = 0.005$ for dmPFC-DRN and $p = 0.0009$ for dmPFC-PAG; two-way repeated-measures ANOVA; Bonferroni multiple comparisons; Figures 3B–3D and 3F–3H), whereas activation of dmPFC-aBLA increased retreats and lowered the tube test rank (day 0, $p < 0.0001$, two-way repeated-measures ANOVA; Bonferroni multiple comparisons post hoc tests; Figures 3J–3L). It should be noted that stimulation of dmPFC-DRN, dmPFC-PAG, or dmPFC-aBLA pathways did not induce either preference or aversion in real-time place-preference tests ($n = 10$, $p = 0.74$ for dmPFC-DRN; $n = 11$, $p = 0.94$ for dmPFC-PAG; and $n = 10$, $p = 0.56$ for dmPFC-aBLA; paired t test).

In addition, by injecting retrograde virus AAV2/2Retro-hSyn-Cre into the DRN, PAG, or aBLA, respectively, and AAV-expressing Cre-inducible light-sensitive ChR2 into the dmPFC (Figures S5A, S5C, and S5E), we specifically activated the DRN-, PAG-, and aBLA-projecting dmPFC neurons. Consistently, we found that the activation of DRN- and PAG-projecting dmPFC neurons increased rank (Figures S5B and S5D), whereas activation of aBLA-projecting dmPFC neurons induced rank drop (Figure S5F). Importantly, stimulation of dmPFC projecting neurons had a similar success rate as terminal stimulations (7/11 for dmPFC-DRN terminal stimulation, 5/7 for DRN-projecting dmPFC neurons stimulation; 7/10 for dmPFC-PAG terminal stimulation, 7/9 for PAG-projecting dmPFC neurons stimulation; and 6/10 for dmPFC-aBLA terminal stimulation, 4/7 for aBLA-projecting dmPFC neurons stimulation; Figures 3B, 3F, and 3J, compare with Figures S5B, S5D, and S5F).

Manipulation of the aBLA also affects tube test rank

As the dmPFC-aBLA pathway showed a distinct role in regulating social competition, to further confirm the function of this

Please cite this article in press as: Xin et al., Deconstructing the neural circuit underlying social hierarchy in mice, Neuron (2024), https://doi.org/10.1016/j.neuron.2024.11.007

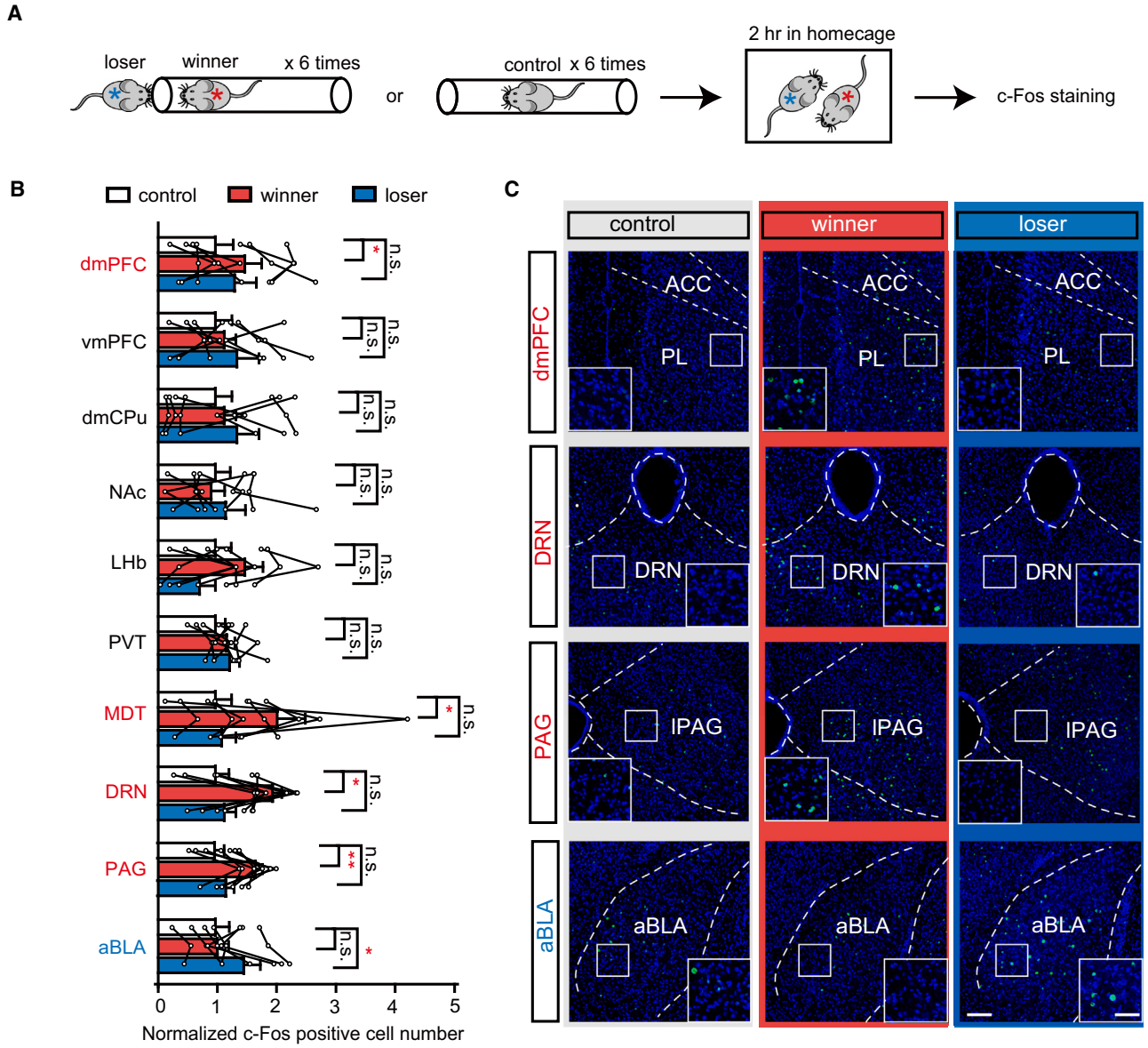

Figure 1. Identification of win- or lose- activated brain regions downstream of the dmPFC

(A) Schematic of behavioral procedure for c-Fos immunohistochemistry experiment. Blue and red stars indicate loser and winner mice, respectively.

(B) Quantification of c-Fos-positive cells in the dmPFC (control vs. winner, $p = 0.02$; control vs. loser, $p = 0.36$), vmPFC (control vs. winner, $p > 0.99$; control vs. loser, $p = 0.57$), and major dmPFC downstream targets including the dmCPu (control vs. winner, $p > 0.99$; control vs. loser, $p > 0.99$), NAc (control vs. winner, $p > 0.99$; control vs. loser, $p = 0.57$), LHb (control vs. winner, $p = 0.22$; control vs. loser, $p = 0.46$), PVT (control vs. winner, $p > 0.99$; control vs. loser, $p = 0.57$), MDT (control vs. winner, $p = 0.02$; control vs. loser, $p > 0.99$), PAG (control vs. winner, $p = 0.003$; control vs. loser, $p = 0.85$), DRN (control vs. winner, $p = 0.03$; control vs. loser, $p > 0.99$), and aBLA (control vs. winner, $p = 0.36$; control vs. loser, $p = 0.02$). $n = 7$ for each control, winner, and loser group. Friedman test with Dunn's multiple comparisons test. Mean ± SEM. $^{*}p < 0.05$, $^{**}p < 0.01$; n.s., not significant.

(C) Representative images of c-Fos-positive cells in the dmPFC and major dmPFC downstream regions including the PAG, DRN, and aBLA from control, winner, and loser mice. Scale bars, 50 μm (inset) and 100 μm.

See also Figure S1 and Table S1.

pathway, we next tried to inhibit or activate the aBLA itself in tube tests (Figure 4). When optogenetically inhibiting the aBLA (Figure 4A), we found that mice displayed more pushes and less retreats and increased dominance rank in seven out of nine mice tested in the tube tests (day 0, $p < 0.0001$, two-way repeated-measures ANOVA; Bonferroni multiple comparisons post hoc tests; Figures 4B–4D). In contrast, acute optogenetic activation of the aBLA decreased tube test rank in seven out of eight mice (day 0, $p < 0.0001$, two-way repeated-measures ANOVA; Bonferroni multiple comparisons; Figures 4E–4H).

Please cite this article in press as: Xin et al., Deconstructing the neural circuit underlying social hierarchy in mice, Neuron (2024), https://doi.org/10.1016/j.neuron.2024.11.007

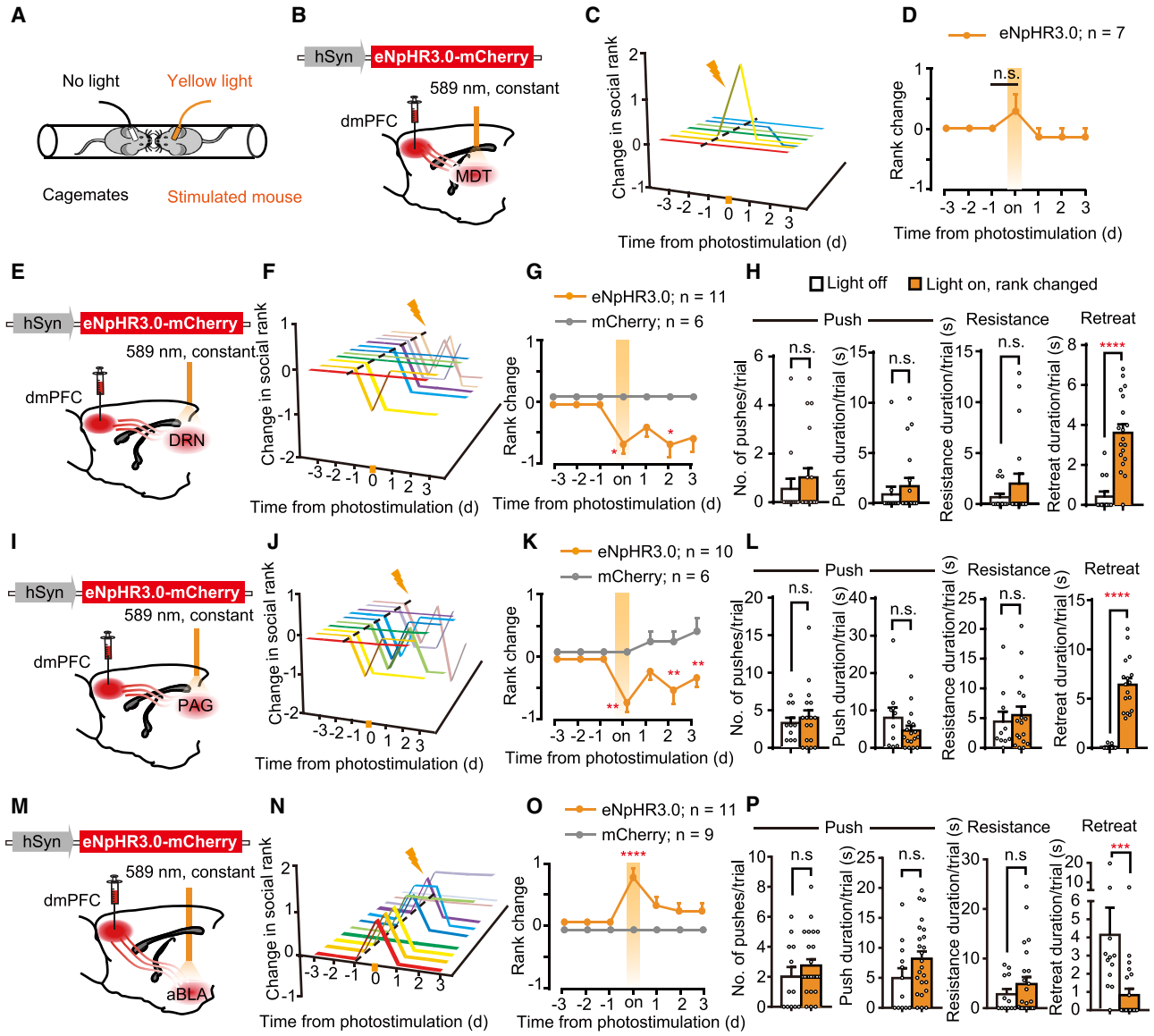

Figure 2. Altered dominance rank by inhibition of different dmPFC downstream circuits

(A) Schematic of optogenetic manipulation during tube test.

(B, E, I, and M) Schematic of AAV-hSyn-eNpHR3.0-mCherry virus construct, viral injection site in the dmPFC, and optic fiber implantation site in dmPFC downstream targets including the MDT (B), DRN (E), PAG (I), and aBLA (M). 589-nm yellow light was delivered constantly during tube test confrontation.

(C, F, J, and N) Summary of rank change in tube test after optogenetic inhibition of dmPFC-MDT (C), dmPFC-DRN (F), dmPFC-PAG (J), or dmPFC-aBLA (N) pathway. Each line represents one animal. Light stimulation was delivered during the tube test on day 0.

(D, G, K, and O) Average rank change after optogenetic inhibition of dmPFC-MDT (D, light on compare with day −1, $n = 7$, $W = 1$, $p > 0.99$), dmPFC-DRN (G, dmPFC-DRN::eNpHR3.0 vs. dmPFC-DRN::mCherry on day 0, $n = 11$ and 6, $p = 0.02$), dmPFC-PAG (K, dmPFC-PAG::eNpHR3.0 vs. dmPFC-PAG::mCherry on day 0, $n = 10$ and 6, $p = 0.003$), or dmPFC-aBLA (O, dmPFC-aBLA::eNpHR3.0 vs. dmPFC-aBLA::mCherry on day 0, $n = 11$ and 9, $p < 0.0001$) pathway. Wilcoxon matched-pairs signed rank test for dmPFC-MDT, and two-way repeated-measures ANOVA with Bonferroni multiple comparisons post hoc tests for dmPFC-DRN, dmPFC-PAG, and dmPFC-aBLA pathways.

(H, L, and P) Behavioral performance of the same mice with or without optogenetic inhibition ($n = 13$ and 19 trials for dmPFC-DRN, $n = 10$ and 17 trials for dmPFC-PAG, $n = 12$ and 24 trials for dmPFC-aBLA). Number of pushes ($U = 105$, $p = 0.37$ for dmPFC-DRN; $U = 82.5$, $p = 0.91$ for dmPFC-PAG; and $U = 108.5$, $p = 0.23$ for dmPFC-aBLA), push duration ($U = 103.5$, $p = 0.34$ for dmPFC-DRN; $U = 62$, $p = 0.26$ for dmPFC-PAG; and $U = 94$, $p = 0.09$ for dmPFC-aBLA), resistance duration ($U = 120$, $p = 0.82$ for dmPFC-DRN; $U = 78$, $p = 0.75$ for dmPFC-PAG; and $U = 130$, $p = 0.63$ for dmPFC-aBLA), and retreat duration ($U = 15$, $p < 0.0001$ for dmPFC-DRN; $U = 0$, $p < 0.0001$ for dmPFC-PAG; and $U = 43.5$, $p = 0.0001$ for dmPFC-aBLA) were compared. Only mice showing rank changes are analyzed. Mann-Whitney U test.

Error bars indicate ± SEM. $^{*}p < 0.05$; $^{**}p < 0.01$; $^{***}p < 0.001$; $^{****}p < 0.0001$; n.s., not significant.

See also Figures S2 and S3 and Table S1.

Please cite this article in press as: Xin et al., Deconstructing the neural circuit underlying social hierarchy in mice, Neuron (2024), https://doi.org/10.1016/j.neuron.2024.11.007

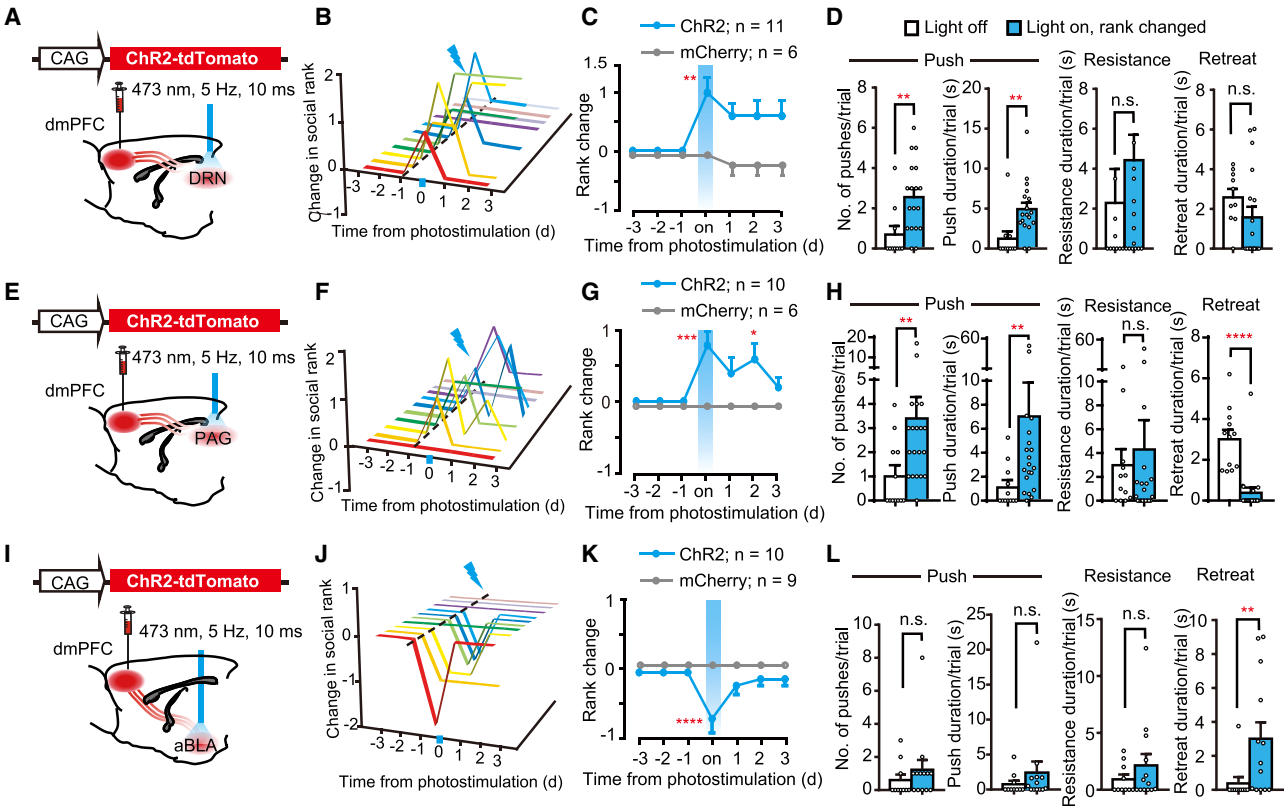

Figure 3. Altered dominance rank by activation of different dmPFC downstream circuits

(A, E, and I) Schematic of AAV-CAG-ChR2-tdTomato virus construct, viral injection site in the dmPFC, and optic fiber implantation site in dmPFC downstream targets, including the DRN (A), PAG (E), and aBLA (I). 473-nm blue light was delivered in 5 Hz, 10 ms during tube test confrontation.

(B, F, and J) Summary of rank change in tube test after optogenetic activation of dmPFC-DRN (B), dmPFC-PAG (F), or dmPFC-aBLA (J) pathway. Each line represents one animal. Light stimulation was delivered during the tube test on day 0.

(C, G, and K) Average rank change after optogenetic activation of dmPFC-DRN (C, dmPFC-DRN::ChR2 vs. dmPFC-DRN::mCherry on day 0, $n = 11$ and 6, $p = 0.005$), dmPFC-PAG (G, dmPFC-PAG::ChR2 vs. dmPFC-PAG::mCherry on day 0, $n = 10$ and 6, $p = 0.0009$), or dmPFC-aBLA (K, dmPFC-aBLA::ChR2 vs. dmPFC-aBLA::mCherry on day 0, $n = 10$ and 9, $p < 0.0001$) pathway. Two-way repeated-measures ANOVA with Bonferroni multiple comparisons post hoc tests.

(D, H, and L) Behavioral performance of the same mice with or without optogenetic activation ($n = 10$ and 18 trials for dmPFC-DRN, $n = 12$ and 20 trials for dmPFC-PAG, $n = 10$ and 13 trials for dmPFC-aBLA). Number of pushes ($U = 32.5$, $p = 0.004$ for dmPFC-DRN; $U = 52$, $p = 0.006$ for dmPFC-PAG; and $U = 49$, $p = 0.29$ for dmPFC-aBLA), push duration ($U = 28$, $p = 0.002$ for dmPFC-DRN; $U = 45$, $p = 0.002$ for dmPFC-PAG; and $U = 48.5$, $p = 0.28$ for dmPFC-aBLA), resistance duration ($U = 61.5$, $p = 0.16$ for dmPFC-DRN; $U = 93.5$, $p = 0.30$ for dmPFC-PAG; and $U = 52$, $p = 0.42$ for dmPFC-aBLA), and retreat duration ($U = 55$, $p = 0.09$ for dmPFC-DRN; $U = 11$, $p < 0.0001$ for dmPFC-PAG; and $U = 27$, $p = 0.009$ for dmPFC-aBLA) were compared. Only mice showing rank changes are analyzed. Mann-Whitney U test.

Error bars indicate ± SEM. $^*p < 0.05$; $^{**}p < 0.01$; $^{***}p < 0.001$; $^{****}p < 0.0001$; n.s., not significant.

See also Figures S3–S5 and Table S1.

Distinct layer-specific subpopulations of dmPFC neurons projecting to different targets

The above set of data suggests that there is functional heterogeneity within the dmPFC neurons for social competition: DRN- and PAG-projecting ones are win related, while aBLA-projecting ones are lose related. To examine whether this difference in function may arise from their differential location within the dmPFC, we injected retrograde tracers into the DRN, PAG, and aBLA to visualize dmPFC neurons that project to each target region (DRN: $n = 1{,}156$ neurons from 5 animals, PAG: $n = 377$ neurons from 7 animals, aBLA: $n = 917$ neurons from 5 animals; Figures S6A–6C). Co-labeling of multi-colored retrograde tracers revealed that the position of aBLA-projecting neurons, which were in layer 2/3, was clearly more medial than those of the DRN- and PAG-neurons, which were in layer 5 (Figures S6D and S6E). Also, there was little overlap at the single-cell level between the aBLA-projecting neurons and the DRN- or PAG-projecting neurons (Figure S6F). Therefore, win-related and lose-related neurons are anatomically segregated in different layers within the dmPFC.

Intriguingly, when we compared c-Fos immunoreactivity patterns after tube tests, between different layers of the dmPFC, winner mice showed increased c-Fos expression in layer 5 ($p = 0.02$, Friedman test with Dunn's multiple comparisons test, Figure S7A). In contrast, a slight increase of c-Fos expression in loser mice was found in layer 2/3 of the dmPFC ($p = 0.07$, Friedman test with Dunn's multiple comparisons test, Figure S7D). When optogenetically activating layer 5

Please cite this article in press as: Xin et al., Deconstructing the neural circuit underlying social hierarchy in mice, Neuron (2024), https://doi.org/10.1016/j.neuron.2024.11.007

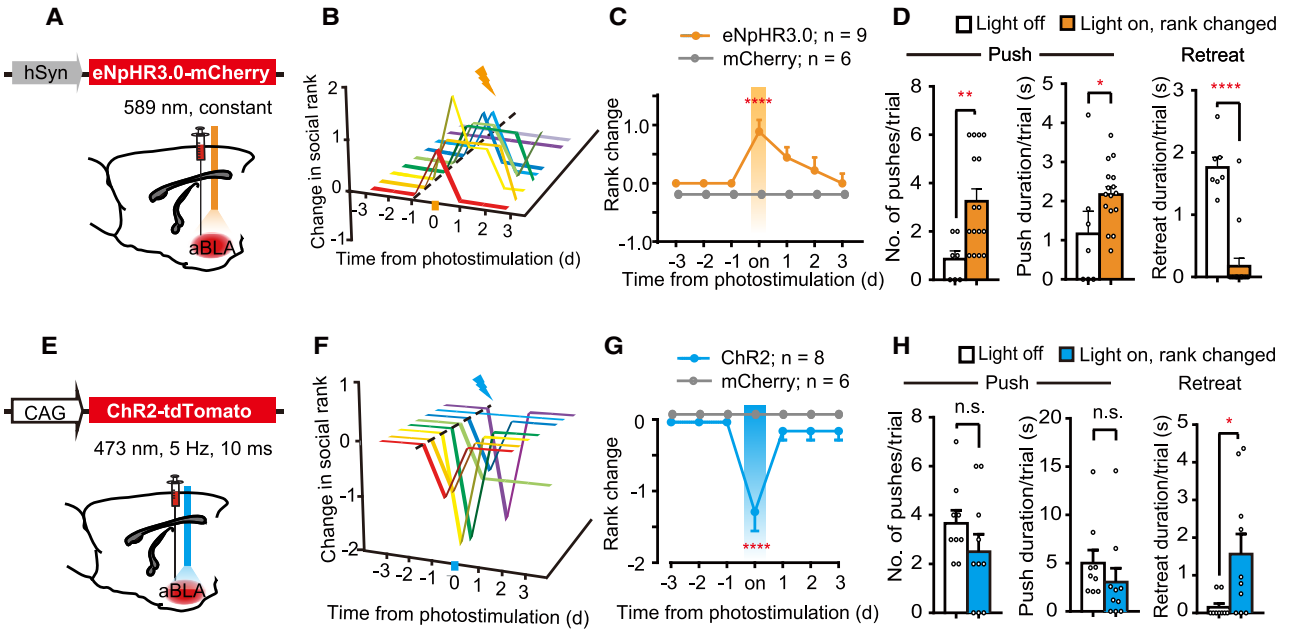

Figure 4. Manipulation of the aBLA also affects tube test rank

(A and E) Schematic of virus construct and viral injection site in the aBLA.

(B and F) Summary of rank change in tube test after optogenetic inhibition (B) or activation (F) of the aBLA. Each line represents one animal.

(C and G) Average rank change after optogenetic inhibition (C, aBLA::eNpHR3.0 vs. aBLA::mCherry, n = 9 and 6, $p < 0.0001$) or activation (G, aBLA::ChR2 vs. aBLA::mCherry, n = 8 and 6, $p < 0.0001$) of the aBLA. Two-way repeated-measures ANOVA with Bonferroni multiple comparisons post hoc tests.

(D and H) Behavioral performance of the same mice with or without optogenetic stimulation (n = 7 and 16 trials for inhibition, n = 9 and 10 trials for activation). Number of pushes (U = 16, $p = 0.006$ for inhibition and U = 28.5, $p = 0.18$ for activation), push duration (U = 25, $p = 0.04$ for inhibition and U = 25, $p = 0.11$ for activation), and retreat duration (U = 4, $p < 0.0001$ for inhibition and U = 18.5, $p = 0.02$ for activation) were compared. Only mice showing rank changes are analyzed. Mann-Whitney U test.

Error bars indicate ± SEM. *$p < 0.05$; **$p < 0.01$; ****$p < 0.0001$; n.s., not significant.

See also Figures S9 and S10 and Table S1.

neurons in Thy1::ChR2 mice, we observed an increase in tube test rank comparable to that of the whole dmPFC activation in Zhou et al.[11] (Figures S7B, 7C, and 7F). Activation of layer 2/3 neurons in Wfs1 (a promoter specific for layer 2/3 expression[45])::ChR2 mice induced a decrease in tube test rank in four out of six mice (Figures S7E and S7F). These results further support a functional segregation of superficial and deep layers within the dmPFC in controlling social competition.

Activity dynamics of different dmPFC projection neuron subpopulations in dominance tube test

To examine how the activity of different dmPFC populations dynamically change during social competition, we monitored their activity in real-time tube test confrontations, using the fiber photometry system (Figures 5A and 5B). AAV-expressing Cre-inducible Ca^{2+} indicator GCaMP6s was injected into the right dmPFC, and retrograde virus AAV2/2Retro-hSyn-Cre was injected into the DRN, PAG, or aBLA. Following viral expression, an optic fiber was implanted 200 μm above the dmPFC injection site for Ca^{2+} signal recording (Figures 5C, 5G, and 5K; see STAR Methods). Similar to those of the whole dmPFC,[46] the Ca^{2+} signals of DRN-projecting dmPFC neurons showed a significant increase after push initiation, with an average signal peak (Z score) of 3.5 ± 0.7 (mean ± SEM, $p < 0.01$, permutation test, n = 170 bouts from 10 mice; Figures 5D and 5E). Consistently, the calcium signals, as measured by area under the curve (AUC), were significantly increased in DRN-projecting dmPFC neurons (p = 0.002, U = 4,143 by bout, p = 0.01, U = 5 by subject, Mann-Whitney U test; Figure 5F). Calcium signal in PAG-projecting dmPFC neurons had a trend to increase but did not reach statistical significance (Z score, 1.9 ± 0.7, mean ± SEM, $p > 0.05$, permutation test, n = 146 bouts from 10 mice, Figures 5H and 5I; p = 0.30, U = 3291 by bout, p = 0.25, U = 15 by subject, Mann-Whitney U test, Figure 5J). In contrast, aBLA-projecting dmPFC neurons decreased activity after push onset, with an average signal trough (Z score) of −1.4 ± 0.3 (mean ± SEM, $p < 0.01$, permutation test, n = 327 bouts from 8 mice, Figures 5L and 5M). The AUC of calcium signals was also decreased in aBLA-projecting dmPFC neurons (p = 0.03, U = 6777 by bout, p = 0.03, U = 5 by subject, Mann-Whitney U test; Figure 5N). This Ca^{2+} dynamic suggests that win-related dmPFC-DRN projection neurons were activated, and lose-related dmPFC-aBLA projection neurons were inhibited during "effortful" pushes in competition.

aBLA-projecting layer 2/3 neurons inhibit layer 5 neurons in the dmPFC

To understand how win- and lose-related dmPFC neurons coordinate their activity to regulate dominance behavior, we explored

Please cite this article in press as: Xin et al., Deconstructing the neural circuit underlying social hierarchy in mice, Neuron (2024), https://doi.org/10.1016/j.neuron.2024.11.007

CellPress

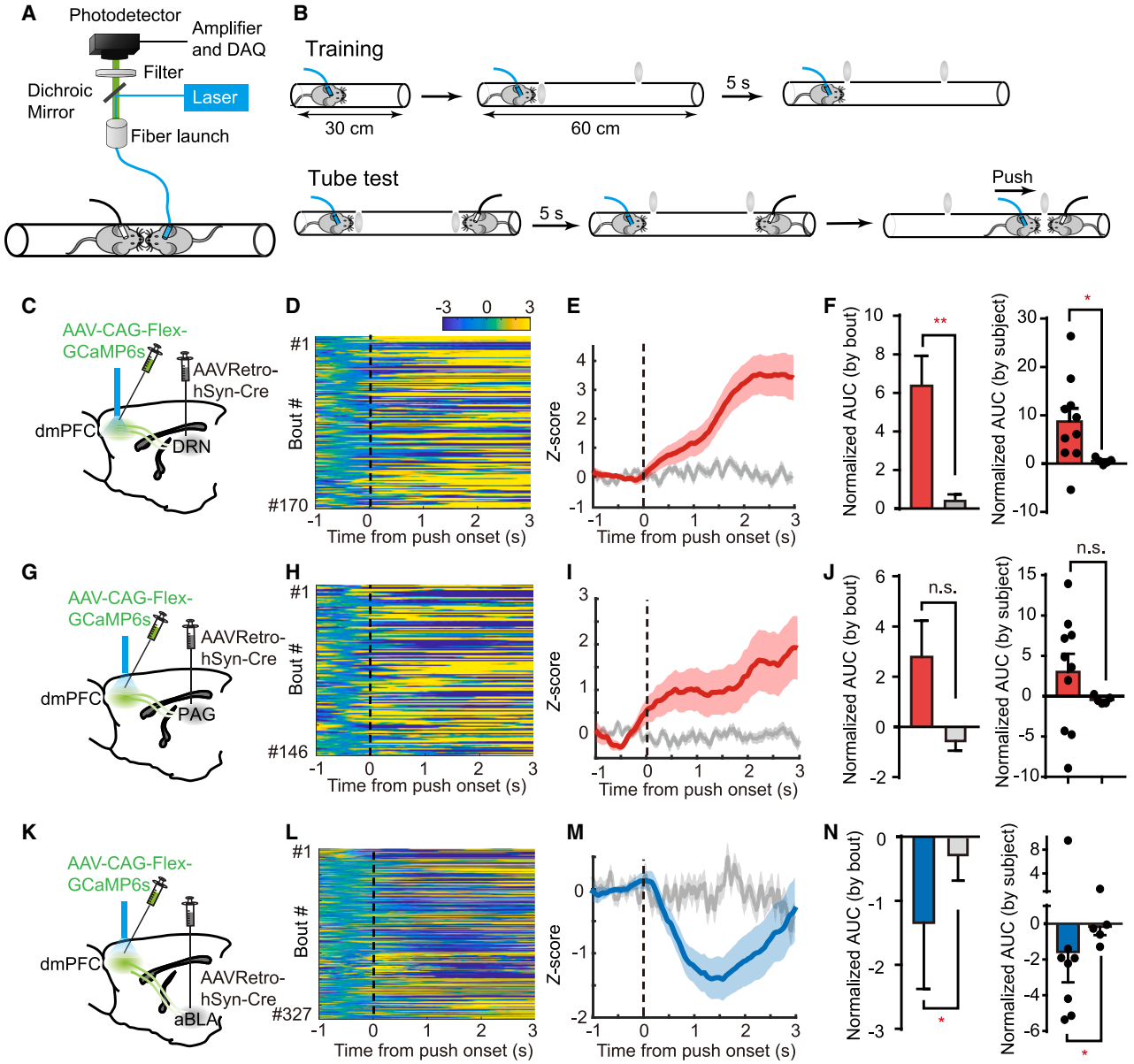

Figure 5. Activity dynamics of different dmPFC projection neuron subpopulations in dominance tube test

(A) Schematic of fiber photometry setup for recording calcium signals of dmPFC projection neurons during tube test confrontation.

(B) Illustration of modified tube test setup and procedures for training (top) and tube test confrontation (bottom). See STAR Methods for details.

(C, G, and K) Schematic illustrating the GCaMP6s viral injection site and optic fiber implantation site for calcium signal recording.

(D, H, and L) Heatmap of *Z* scored Ca^{2+} signals of DRN-projecting (D, $n = 170$ bouts from $N = 10$ mice), PAG-projecting (H, $n = 146$ bouts from $N = 10$ mice), and aBLA-projecting (L, $n = 327$ bouts from $N = 8$ mice) neurons in the dmPFC when mice execute pushes during tube test. Signals are aligned to the time point of push initiation.

(E, I, and M) Peri-event plot of *Z* scored dmPFC Ca^{2+} signals during push in mice expressing GCaMP6s (in red or blue) or EYFP (in gray). Signals are aligned to push initiation. Thick lines indicate the mean, and shaded areas indicate the SEM.

(F, J, and N) Normalized AUC of *Z* scored Ca^{2+} signals of DRN-projecting (F, by bout: $n = 170$ and 66, U = 4,143, $p = 0.002$; by subject: $N = 10$ and 5, U = 5, $p = 0.01$), PAG-projecting (J, by bout: $n = 146$ and 50, U = 3,291, $p = 0.30$; by subject: $N = 10$ and 5, U = 15, $p = 0.25$), and aBLA-projecting (N, by bout: $n = 327$ and 51, U = 6,777, $p = 0.03$; by subject: $N = 8$ and 5, U = 5, $p = 0.03$) neurons in the dmPFC in mice expressing GCaMP6s (in red or blue) or EYFP (in gray). Mann-Whitney U test. Error bars indicate ± SEM. $^*p < 0.05$; $^{**}p < 0.01$; n.s., not significant.

See also Table S1.

Please cite this article in press as: Xin et al., Deconstructing the neural circuit underlying social hierarchy in mice, Neuron (2024), https://doi.org/10.1016/j.neuron.2024.11.007

how they interact with each other within the dmPFC (Figure 6). We optogenetically activated the win-related, DRN-projecting neurons at layer 5 while performing *in vivo* single-unit recording in layer 2/3, where lose-related, aBLA-projecting neurons are located (Figure 6A). Among the 104 wide-spike, putative pyramidal (pPYR) layer 2/3 neurons recorded, 26% showed a small significant activation, and 10% showed inhibition upon stimulation of DRN-projecting dmPFC neurons (Figure 6D). Overall, the pPYR activity in layer 2/3 was not significantly changed (p = 0.76, paired t test; Figures 6B and 6C). Similarly, an insignificant impact was found on the neural activity of these dmPFC layer 2/3 neurons by optogenetic inhibition of win-related DRN-projecting neurons (Figures 6E–6H). Notably, a much larger effect was observed when we examined the impact in the opposite direction, by optogenetically activating lose-related, aBLA-projecting layer 2/3 neurons and recording layer 5 neurons, where win-related, DRN- and PAG-projecting neurons are located (Figure 6I). Among the 100 pPYR layer 5 neurons recorded, a large fraction (75%) was inhibited, and 6% were activated, upon stimulation of aBLA-projecting neurons (Figure 6L). Overall, pPYR activity in layer 5 was significantly decreased ($p < 0.0001$, paired t test; Figures 6J and 6K). Conversely, when aBLA-projecting neurons were optogenetically inhibited, among the 92 layer 5 pPYR neurons, 62% were activated in the dmPFC layer 5 and only 6% were inhibited (Figure 6P). Overall, pPYR activity in layer 5 was significantly increased ($p < 0.0001$, paired t test; Figures 6N and 6O). These results suggest that lose-related, aBLA-projecting layer 2/3 neurons can potentially inhibit win-related layer 5 neurons in the dmPFC.

Lose-related neurons inhibit win-related neurons through GABAergic interneurons within the dmPFC

To understand the cellular mechanism by which lose-related neurons may inhibit the win-related neurons, we performed brain slice recording experiments (Figure 7). AAV-expressing Cre-inducible light-sensitive ChR2 was injected into the dmPFC, and retrograde virus AAV2/2Retro-hSyn-Cre was injected into the aBLA to express ChR2 tagged with EGFP in aBLA-projecting neurons. DRN-projecting neurons were visualized in red fluorescence by injection of retrograde virus AAV2/2RetroPlus-hSyn-tdTomato-WPRE-pA into the DRN. We then used blue light pulses (5 ms pulse width) to stimulate aBLA-projecting neurons in acute slices while recording from DRN-projecting neurons using whole-cell patch-clamp technique (Figure 7A; see STAR Methods). Photostimulation of aBLA-projecting neurons induced in DRN-projecting neurons biphasic synaptic responses, comprising an early evoked excitatory postsynaptic current (eEPSC) component and a delayed evoked inhibitory postsynaptic current (eIPSC) component (Figure 7B). Notably, the amplitudes of eIPSCs were larger than those of eEPSCs in a large fraction (73%) of DRN-projecting neurons (Figure 7B). Light-evoked EPSCs were completely blocked by application of tetrodotoxin (TTX) and recovered by application of TTX + 4AP (4-aminopyridine, Figure 7C), indicating that the eEPSCs were mediated by direct synaptic connections. On the other hand, light-evoked IPSCs were also completely blocked by application of TTX but not recovered by application of TTX + 4AP (Figure 7D), indicating that the eIPSCs were poly-synaptic inhibitory currents. Furthermore, $GABA_A$ receptor antagonist picrotoxin (PTX) blocked the eIPSCs (Figure 7E).

In order to directly test which population of interneurons mediates the feedforward inhibition from layer 2/3 to layer 5 neurons, we inhibited two major inhibitory interneurons, parvalbumin (PV) or somatostatin (SST), respectively, while monitoring the synaptic responses of layer 5 neurons in response to stimulation of aBLA-projecting dmPFC neurons (Figure S8). For this experiment, we injected pAAV-Ef1a-DIO-eNpHR3.0-mCherry into the dmPFC of PV-Cre or SST-Cre mice. In the same mice, we also injected rAAV2/9-nEF1α-FDIO-hChR2(H134R)-EYFP into the dmPFC and retrograde virus AAV2/2Retro-hSyn-Flpo-WPRE-pA into the aBLA to express ChR2 in aBLA-projecting neurons (Figures S8A and S8E). In brain slices prepared from these mice, yellow light was applied to suppress PV or SST neurons, and blue light was used to stimulate aBLA-projecting dmPFC neurons while synaptic responses of layer 5 were recorded (Figures S8B and S8F). Inhibition of either PV or SST interneurons greatly reduced the feedforward inhibitory currents (PV neurons, 47.0% reduction, n = 12, p = 0.003; SST neurons, 40.3% reduction, n = 11, p = 0.002, one-way repeated-measures ANOVA; Bonferroni multiple comparisons post hoc tests; Figures S8D and S8H). These effects were reversible upon cessation of yellow light illumination (Figures S8C, S8D, S8G, and S8H). These results suggest that both SST and PV interneurons contribute to the feedforward inhibition from layer 2/3 to layer 5 neurons in the dmPFC.

DISCUSSION

In this study, we dissected the individual contribution and reciprocal interaction of dmPFC downstream circuits in modulating dominance behavior. Brain-wide c-Fos mapping experiment revealed that winner mice in the tube test competition exhibited a significantly higher number of c-Fos-positive neurons in the dmPFC downstream targets, including the DRN and PAG, whereas loser mice exhibited more c-Fos-positive neurons in the aBLA. Consistently, pathway-specific manipulations outlined a dmPFC-centric social dominance neural network, in which the dmPFC-DRN and dmPFC-PAG circuits act as win-related pathways, whereas the dmPFC-aBLA circuit acts as a lose-related pathway. Moreover, the activation or inhibition of the aBLA itself yielded similar effects as manipulation of the dmPFC-aBLA pathway. Accordingly, these win- and lose-related dmPFC circuits showed opposing calcium activities when mice initiated "effortful" push behaviors in the tube test competition. Retrograde tracing study revealed that these functionally divergent pathways are anatomically segregated, with the lose-related aBLA-projecting neurons located in the layer 2/3 and the win-related DRN- and PAG- projecting neurons located in the layer 5 of the dmPFC. Finally, using *in vivo* and *in vitro* electrophysiological recordings, we found an inhibition from the lose-related neurons to the win-related neurons through local PV and SST interneurons in the dmPFC. Through such delicate functional organization, the dmPFC coordinates different downstream targets to orchestrate competitive behaviors.

Please cite this article in press as: Xin et al., Deconstructing the neural circuit underlying social hierarchy in mice, Neuron (2024), https://doi.org/10.1016/j.neuron.2024.11.007

CellPress

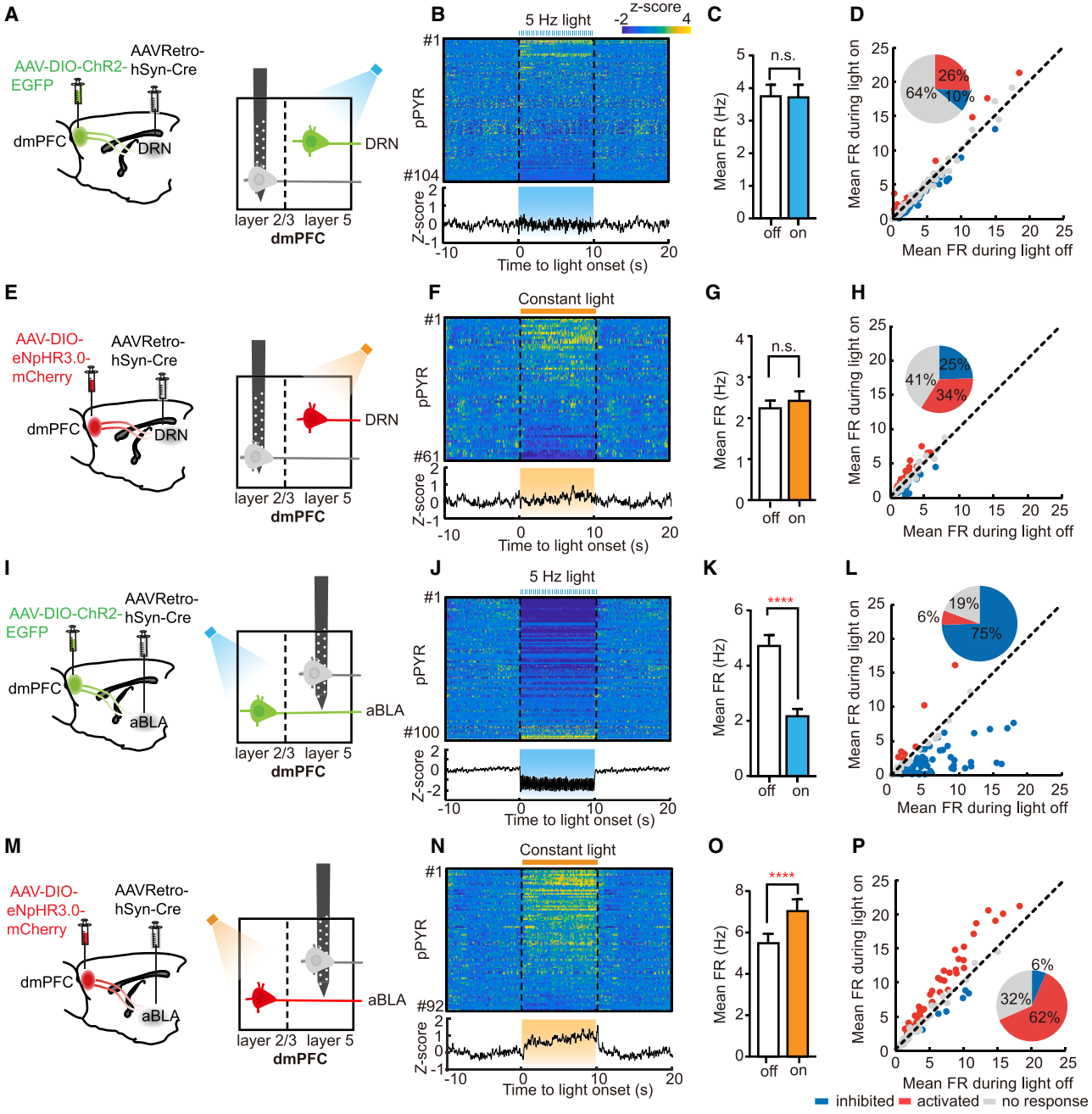

Figure 6. aBLA-projecting layer 2/3 neurons inhibit layer 5 neurons in the dmPFC

(A, E, I, and M) On the left, schematic illustrating the virus and injection site for *in vivo* recording. On the right, schematic illustrating the photostimulation and recording position.

(B, F, J, and N) Peri-stimulus time histograms (PSTHs) of the *Z* score of all recorded neurons. Putative PYR neurons are ranked by ascending (J) or descending (B, F, and N) order of firing rate during the 10 s light-on period. Vertical dashed lines delineate the time when the 10-s stimulation protocol started and ended (top). Average PSTH of the *Z* score of all pPYR units (bottom).

(C, G, K, and O) Comparison of mean firing rate of layer 2/3 neurons (dmPFC-DRN::ChR2, $n = 104$ neurons from $N = 10$ mice, $p = 0.76$; dmPFC-DRN::eNpHR3.0, $n = 61$ neurons from $N = 5$ mice, $p = 0.21$) and layer 5 neurons (dmPFC-aBLA::ChR2, $n = 100$ neurons from $N = 7$ mice, $p < 0.0001$; dmPFC-aBLA::eNpHR3.0, $n = 92$ neurons from $N = 5$ mice, $p < 0.0001$) during 10-s light-off and 10-s light-on epochs. Paired t test. Error bars indicate ± SEM. ****$p < 0.0001$; n.s., not significant.

(D, H, L, and P) Scatterplots of mean firing rate of all neurons during light-off epoch against light-on epoch. Colored circles indicate units that were significantly inhibited (blue), activated (red), or no response (gray) during the light stimulation. Inset pie graphs show the percentage of neurons that were significantly inhibited (blue), activated (red), or no response (gray) during the light stimulation.

See also Figures S6 and S7 and Table S1.

Please cite this article in press as: Xin et al., Deconstructing the neural circuit underlying social hierarchy in mice, Neuron (2024), https://doi.org/10.1016/j.neuron.2024.11.007

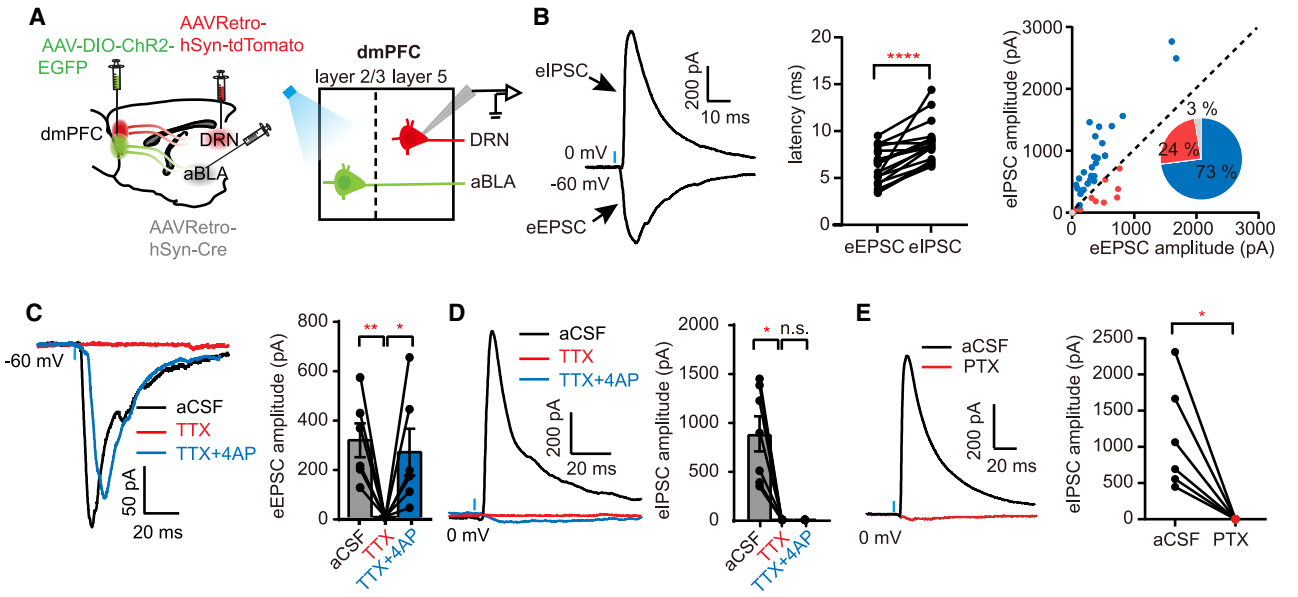

Figure 7. Lose-related neurons inhibit win-related neurons through GABAergic interneurons within the dmPFC

(A) On the left, schematic illustrating the virus and injection site for *in vitro* recording. On the right, schematic illustrating the positions of photostimulation and recording.

(B) Light-evoked IPSCs and EPSCs recorded at 0 and −60 mV holding potential, respectively. On the left, representative traces showing that photostimulation of aBLA-projecting dmPFC neurons elicited in DRN-projecting neurons eEPSCs and eIPSCs, respectively. In the middle, the eIPSCs exhibit higher onset latency than the eEPSCs ($n = 22$, $p < 0.0001$, paired t test). On the right, scatterplots of the amplitude of eIPSCs plotted against the amplitude of eEPSCs. Inset pie graph showing the percentage of neurons larger in eIPSCs than eEPSCs (blue), larger in eEPSCs than eIPSCs (red), or no response (gray) during the light stimulation.

(C) eEPSCs were blocked after bath application of tetrodotoxin (TTX, a voltage-gated Na^+ channel blocker) and recovered after co-application of 4-aminopyridine (4AP, potassium channel blocker). On the left, representative traces of light-evoked EPSCs. On the right, quantification of eEPSC amplitude ($n = 6$, aCSF vs. TTX, $p = 0.008$; TTX vs. TTX + 4AP, $p = 0.04$, Friedman test with Dunn's multiple comparisons test).

(D) eIPSCs were blocked after bath application of TTX and not recovered after co-application of 4AP. On the left, representative traces of light-evoked IPSCs. On the right, quantification of eIPSC amplitude ($n = 7$, aCSF vs. TTX, $p = 0.03$; TTX vs. TTX + 4AP, $p = 0.85$, Friedman test with Dunn's multiple comparisons test).

(E) eIPSCs were blocked by $GABA_A$ receptor antagonist picrotoxin (PTX). On the left, representative traces of light-evoked IPSCs. On the right, quantification of eIPSC amplitude ($n = 6$, $p = 0.03$, Wilcoxon matched-pairs signed rank test).

See also Figures S6–S8 and Table S1.

Role of BLA in regulating dominance hierarchy

As one of the amygdaloid subnuclei, the BLA is well known for regulating fear response[47,48] and shares reciprocal connections with the mPFC.[20,49] The mPFC-BLA connections have been demonstrated to participate in the regulation of fear learning,[50] anxiety,[51] decision-making,[52] social approach-avoidance behavior,[34] and observational learning.[35–37] On the other hand, imaging and recording studies in human and monkey have also indicated that the amygdala codes social rank information. Amygdalar neurons respond more strongly to highly ranked monkey.[53] Viewing facial images of higher social-ranked individuals also resulted in higher activity in the human amygdala.[54] When social hierarchy becomes unstable, the amygdala is activated together with the mPFC.[6] In this study, we found that optogenetic inhibition of the dmPFC-aBLA pathway or the aBLA increased social rank (Figures 2 and 4), whereas their activation decreased rank (Figures 3 and 4), suggesting that this pathway may mediate losing or subordination. This is consistent with a previous study showing that activation of the circuitry from the PL of the PFC to the BLA reduces social investigation and elicits aversion.[34] On the other hand, it should be noted that there is a high degree of heterogeneity within the BLA: the anterior and posterior BLA have been reported to code negative and positive valences, respectively.[55,56] A recent study, through chemogenetic manipulation of a more posterior site in the BLA (pBLA), found that inhibition of the pBLA resulted in a reduction of social rank.[36] To verify the difference between aBLA and pBLA in regulating social dominance, we chemogenetically inhibited the aBLA and pBLA, respectively, during tube test (Figure S9; see STAR Methods and also Figure S10). We found that after inhibition of the aBLA with CNO (5 mg/kg), mice displayed less retreats and increased dominance rank (0.5 h, $p = 0.001$; 1.5 h, $p < 0.0001$; 6 h, $p = 0.02$, two-way repeated-measures ANOVA; Bonferroni multiple comparisons; Figures S9A–S9D), which is consistent with our results of optogenetic inhibition (Figure 4). On the other hand, for the inhibition of the pBLA, consistent with reports from Scheggia et al.,[36] mice displayed more retreats and decreased dominance rank after treatment with CNO (0.5 h, $p = 0.03$; 1.5 h, $p = 0.0002$; 6 h, $p = 0.03$; 48 h, $p = 0.003$; two-way repeated-measures ANOVA; Bonferroni multiple comparisons; Figures S9E–S9H). Therefore, it is likely that the anterior and posterior subdivisions of the BLA may play opposite roles in regulating social dominance. This heterogeneity may also account for some

Please cite this article in press as: Xin et al., Deconstructing the neural circuit underlying social hierarchy in mice, Neuron (2024), https://doi.org/10.1016/j.neuron.2024.11.007

controversial outcomes from early amygdaloid lesion studies, with some studies finding that amygdala lesions resulted in a loss of dominance status,[57] whereas others found that they resulted in an increase in dominance display and elevated confidence in social interactions.[58,59] Such functional divergence may potentially be explained by the antagonistic interaction between the distinct valence-encoding neurons.[55,56]

Role of DRN in regulating dominance hierarchy

DRN is a major source of serotonin, which has been extensively studied in the establishment and maintenance of social status in crustaceans[60] and aggressiveness in vertebrates.[61–63] The PFC-DRN pathway in mice has been implicated in regulating behavioral control over aversive challenges.[30,64,65] Notably, selectively activation of dmPFC axons in the DRN instantaneously induced effortful behavioral response to challenging conditions.[30] Consistently, here we found that activation of the dmPFC-DRN pathway induced more pushes and winning in tube test competition (Figure 3). This result suggests that the strength of the dmPFC-DRN pathway may encode a dominance-associated personality trait such as motivational drive or perseverance in social confrontations.

Although the DRN is the predominant serotonergic source, it is not a homogeneous nucleus. It also contains other cell types including GABAergic and glutamatergic neurons,[66] although the mPFC sends biased input to the serotoninergic type.[67] There are also considerable heterogeneity within serotonergic neurons in the DRN with respect to molecular identity, physiological property, and connectivity.[66,68,69] Future studies are necessary to dissect more precisely the function of each cell type and individual subpopulation of serotonin neurons within the DRN in regulating social competition.

Role of PAG in regulating dominance hierarchy

PAG has been strongly implicated in defensive behaviors. *In vivo* electrophysiological recordings have identified fighting-responsive neurons in the PAG.[70] Electrical stimulation of the PAG induced aggressive behaviors,[71,72] while silencing this area blocked the expression of defensive rage.[73,74] The PAG contains four longitudinal columns, referred to as the dorsomedial (dmPAG), dorsolateral (dlPAG), lateral (lPAG), and ventrolateral (vlPAG) subdivisions, which collectively play a pivotal role in the coordination of defensive action,[75] with the dorsal PAG (dPAG) and lPAG modulating active defensive responses and the vlPAG modulating passive defensive responses.[76–79] The dmPFC projects densely to the dlPAG and lPAG regions[80] (Figure S1). Stimulation of the mPFC-dPAG circuit elicited defensive behaviors,[81] while inhibition of this circuit mimicked the effect of social defeat.[17] Consistently, we have found here that inhibition of the dmPFC-PAG pathway induced losing in the tube test competition (Figure 2). We thus speculate that during social confrontation, the dmPFC works through the PAG to elevate aggressiveness and to generate defensive pushes.

Role of other dmPFC downstream pathways in regulating dominance hierarchy

Among other downstream targets of the dmPFC, the NAc has been shown to play an important role in social competition. Human neuroimaging data revealed that neural activity in the NAc increases when subjects view a photograph of a higher-ranked opponent.[6] Subordinate mice show lower levels of energy-related metabolites in the NAc than dominant ones.[82] Mitochondrial function of the NAc regulates the establishment of social hierarchy, particularly the influence of anxiety on social competitiveness.[83,84] In a recent study, Choi et al.[40] showed that mice with genetically ablated mPFC-NAc projection were significantly more prone to lose. In the current study, we did not find optogenetic inhibition of the dmPFC-NAc pathway during the tube test affecting social rank (Figure S2). One possible interpretation is that the chronic energy metabolism of the NAc is required for the establishment of a dominance rank, and a transient inhibition of dmPFC-NAc pathway is insufficient to induce instantaneous losing. Another possible interpretation may be the functional divergency of NAc subdivisions.[85] The NAc can be divided into the core and shell,[86] both of which receive projections from the mPFC.[20] According to their brain images and surgery coordinates, Choi et al.[40] preferentially targeted the medial part of the NAc, potentially including the medial shell and part of the medial part of NAc core. In our study, we targeted the more lateral part of the NAc. In addition, since D1 MSNs in the shell and D2 MSNs in the core play opposite roles in modulating social dominance,[87] it is also possible that when we generally inhibited the dmPFC-NAc pathway, the effects on the D1 and D2 may cancel out each other. Finally, the difference in the anterior-posterior coordinates of the mPFC could also be a potential cause for the discrepancy.

The dmPFC also strongly innervates the striatum (dmCPu, Figure S1), which is known to be involved in decision-making,[26] particularly when being rewarded socially.[88] Although we did not find a significant effect on tube test rank when inhibiting the dmPFC-dmCPu pathway, given the rewarding property of winning, it is possible that this pathway is not directly involved in regulating social rank but instead involved in the reinforcement of winning in social competition.

Function of different dmPFC layers in social dominance

Different from the traditional laminar view, the mPFC lacks a canonical thalamo-recipient layer 4, with inputs arriving across layer 1 to layer 6.[22] Besides, projection neurons in the mPFC span across layer 2 to layer 6 and target divergent brain regions. While consistent with previous literature that a majority of dmPFC-aBLA neurons reside in superficial layer 2/3, and dmPFC-DRN and dmPFC-PAG neurons reside in deeper layer 5[21] (Figure S6), it is intriguing to find that these layer-segregated, projection-specific neurons function oppositely in social competition, with the layer 2/3 neurons mediating subordination and layer 5 neurons mediating dominance (Figure S7). Consistent with such heterogeneity, while we found that dominant mice have a higher excitatory synaptic strength in dmPFC layer 5 pyramidal neurons than subordinate cagemates,[8,89] Tada et al. found that dmPFC layer 2/3 neurons exhibit reduced synaptic strength in social-isolation-induced dominant rats.[90] Thus, our study shows that even within a specific brain region, there can be highly heterogeneous function in different projection-specific cells located in different layers.

Please cite this article in press as: Xin et al., Deconstructing the neural circuit underlying social hierarchy in mice, Neuron (2024), https://doi.org/10.1016/j.neuron.2024.11.007

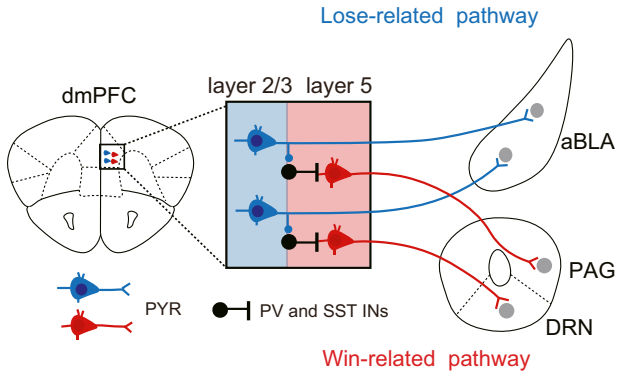

Figure 8. Working model

Schematic illustrating lose-related aBLA-projecting neurons located in the layer 2/3 inhibiting win-related DRN- and PAG-projecting neurons located in the layer 5 of the dmPFC through local PV and SST inhibitory neurons.

A tug of war between dmPFC layers

The canonical flow of information between cortical layers is considered to orient from thalamo-recipient layer 4 to layer 2/3, which then signals to layer 5.[91] In the mPFC, despite a lack of layer 4, there is also a hierarchy of connectivity from superficial to deep layers.[22] Interestingly, cortico-amygdalar neurons located in layer 2/3 of the mPFC exclusively target pyramidal tract (PT) neurons in layer 5,[92] which then project to various subcortical areas such as PAG and DRN. Previously, *in vitro* experiments have been performed on brain slices to test the functional impact of layer 2/3 projections onto layer 5. It was found that activation of layer 2/3 neurons drives direct excitation combined with feedforward inhibition in layer 5 neurons in the somatosensory cortex,[93] as well as in the mPFC.[92] Specifically, compared with those in the barrel cortex, layer 5 neurons in the mPFC received a substantially larger fraction of local inhibitory inputs.[94] When measured excitatory conductance and inhibitory conductance were injected into layer 5 PT neurons of the mPFC to mimic layer 2/3 inputs, excitatory-conductance-evoked spiking can be significantly attenuated by simultaneous injection of inhibitory conductance.[92] These findings indicate that information flow from layer 2/3 to layer 5 can be strongly shaped by local inhibitory circuits in the mPFC. However, prior to the present study, it was not well understood what the global impact is of layer 2/3 inputs on layer 5 neurons in the mPFC *in vivo*.

Here, by combining *in vivo* and *in vitro* electrophysiological recordings, we discovered that layer 2/3 neurons in general inhibit layer 5 neurons in the dmPFC, through local PV and SST interneurons (Figures 6, 7, and S8). As a result, layer-2/3-locating, lose-related pathway could inhibit the layer-5-locating, win-related pathway (Figure 8). One interesting speculation of the function of this unidirectional interaction is that losing mentality may dominate over winning during competitions: once animals initiate the idea of quitting or withdrawing from the rivalry, the inhibition on the win pathway from the lose pathway would help them execute the idea and end the fight quickly. In addition to regulating dominance behavior, this newly discovered unidirectional interlaminar inhibition may also play important functions in other behavioral controls involving the mPFC.

RESOURCE AVAILABILITY

Lead contact

Requests for further information and for resources and reagents may be directed to and will be fulfilled by the lead contact, Hailan Hu (huhailan@zju.edu.cn).

Materials availability

This study did not generate new unique reagents.

Data and code availability

- All data reported in this paper will be shared by the lead contact upon request.
- This paper does not report original code.
- Any additional information required to reanalyze the data reported in this paper is available from the lead contact upon request.

ACKNOWLEDGMENTS

We thank Jingxiang Tang, Yang Xiong, Pinyi Wu, Hui Zhao, Xiaoqi Wang, Qinglin Fan, Youguang Wang, and colleagues from Hu lab for assistance in experiments and Xinkuan Xiang and Haohong Li for advice on *in vivo* recording. Some graphic components were created with BioRender. This work was supported by the National Natural Science Foundation of China (32130042 and 82288101), the STI2030-Major Projects (2021ZD0203000 and 2021ZD0203001), the Starry Night Science Fund of Zhejiang University Shanghai Institute for Advanced Study (SN-ZJU-SIAS-002), the New Cornerstone Science Foundation, Key R&D Program of Zhejiang (2024SSYS0016), and the Project for Hangzhou Medical Disciplines of Excellence and Key Project for Hangzhou Medical Disciplines to H.H.

AUTHOR CONTRIBUTIONS

H.H., Q.X., and T.Z. designed the study. Q.X., D.Z., and J.X. performed c-Fos immunohistochemistry experiments. Q.X. and J.X. performed anterograde and retrograde tracing experiments. Q.X., T.Z., D.Z., and J.X. performed optogenetic and chemogenetic manipulations and related behavioral analysis. Q.X. and J.X. performed fiber photometry recording experiments. Q.X. performed *in vivo* recording experiments. D.Z. and T.Z. performed *in vitro* recording experiments. Z.N. assisted Q.X. in analyzing photometry and *in vivo* recording data. H.H. and Q.X. wrote the manuscript.

DECLARATION OF INTERESTS

H.H. is a member of the advisory board of *Neuron*.

DECLARATION OF GENERATIVE AI AND AI-ASSISTED TECHNOLOGIES IN THE WRITING PROCESS

During the preparation of this work, the authors used ChatGPT to check grammar and spelling. After using this tool, the authors reviewed and edited the content as needed. No generative AI tools have been used to produce any new content. The authors take full responsibility for the content of the publication.

STAR★METHODS

Detailed methods are provided in the online version of this paper and include the following:

- KEY RESOURCES TABLE
- EXPERIMENTAL MODEL AND STUDY PARTICIPANT DETAILS
  - Animals
- METHOD DETAILS
  - Tube test
  - c-Fos immunohistochemistry staining
  - Stereotactic surgeries

- Optogenetic and chemogenetic manipulations in tube test
- RTPP test
- Fiber photometry recording in tube test
- Anterograde and retrograde tracing
- *In vivo* electrophysiological recording in head-fixed mice
- *In vitro* electrophysiological recording

- QUANTIFICATION AND STATISTICAL ANALYSIS

SUPPLEMENTAL INFORMATION

Supplemental information can be found online at https://doi.org/10.1016/j.neuron.2024.11.007.

Received: March 11, 2024
Revised: August 29, 2024
Accepted: November 11, 2024
Published: December 10, 2024

REFERENCES

1. Zhou, T., Sandi, C., and Hu, H. (2018). Advances in understanding neural mechanisms of social dominance. Curr. Opin. Neurobiol. *49*, 99–107. https://doi.org/10.1016/j.conb.2018.01.006.
2. Watanabe, N., and Yamamoto, M. (2015). Neural mechanisms of social dominance. Front. Neurosci. *9*, 154. https://doi.org/10.3389/fnins.2015.00154.
3. Chen, P., and Hong, W. (2018). Neural circuit mechanisms of social behavior. Neuron *98*, 16–30. https://doi.org/10.1016/j.neuron.2018.02.026.
4. Coley, A.A., Padilla-Coreano, N., Patel, R., and Tye, K.M. (2021). Valence processing in the PFC: Reconciling circuit-level and systems-level views. Int. Rev. Neurobiol. *158*, 171–212. https://doi.org/10.1016/bs.irn.2020.12.002.
5. Ligneul, R., Obeso, I., Ruff, C.C., and Dreher, J.C. (2016). Dynamical representation of dominance relationships in the human rostromedial prefrontal cortex. Curr. Biol. *26*, 3107–3115. https://doi.org/10.1016/j.cub.2016.09.015.
6. Zink, C.F., Tong, Y., Chen, Q., Bassett, D.S., Stein, J.L., and Meyer-Lindenberg, A. (2008). Know your place: neural processing of social hierarchy in humans. Neuron *58*, 273–283. https://doi.org/10.1016/j.neuron.2008.01.025.
7. Sallet, J., Mars, R.B., Noonan, M.P., Andersson, J.L., O'Reilly, J.X., Jbabdi, S., Croxson, P.L., Jenkinson, M., Miller, K.L., and Rushworth, M.F. (2011). Social network size affects neural circuits in macaques. Science *334*, 697–700. https://doi.org/10.1126/science.1210027.
8. Wang, F., Zhu, J., Zhu, H., Zhang, Q., Lin, Z.M., and Hu, H.L. (2011). Bidirectional control of social hierarchy by synaptic efficacy in medial prefrontal cortex. Science *334*, 693–697. https://doi.org/10.1126/science.1209951.
9. Padilla-Coreano, N., Batra, K., Patarino, M., Chen, Z.X., Rock, R.R., Zhang, R.H., Hausmann, S.B., Weddington, J.C., Patel, R., Zhang, Y.E., et al. (2022). Cortical ensembles orchestrate social competition through hypothalamic outputs. Nature *603*, 667–671. https://doi.org/10.1038/s41586-022-04507-5.
10. Li, S.W., Zeliger, O., Strahs, L., Báez-Mendoza, R., Johnson, L.M., Wojciechowski, A.M., and Williams, Z.M. (2022). Frontal neurons driving competitive behaviour and ecology of social groups. Nature *603*, 661–666. https://doi.org/10.1038/s41586-021-04000-5.
11. Zhou, T., Zhu, H., Fan, Z., Wang, F., Chen, Y., Liang, H., Yang, Z., Zhang, L., Lin, L., Zhan, Y., et al. (2017). History of winning remodels thalamo-PFC circuit to reinforce social dominance. Science *357*, 162–168. https://doi.org/10.1126/science.aak9726.
12. Wang, F., Kessels, H.W., and Hu, H.L. (2014). The mouse that roared: neural mechanisms of social hierarchy. Trends Neurosci. *37*, 674–682. https://doi.org/10.1016/j.tins.2014.07.005.
13. Zhu, H., and Hu, H.L. (2018). Brain's neural switch for social dominance in animals. Sci. China Life Sci. *61*, 113–114. https://doi.org/10.1007/s11427-017-9181-1.
14. Padilla-Coreano, N., Tye, K.M., and Zelikowsky, M. (2022). Dynamic influences on the neural encoding of social valence. Nat. Rev. Neurosci. *23*, 535–550. https://doi.org/10.1038/s41583-022-00609-1.
15. Ferreira-Fernandes, E., and Peça, J. (2022). The neural circuit architecture of social hierarchy in rodents and primates. Front. Cell. Neurosci. *16*, 874310. https://doi.org/10.3389/fncel.2022.874310.
16. Dwortz, M.F., Curley, J.P., Tye, K.M., and Padilla-Coreano, N. (2022). Neural systems that facilitate the representation of social rank. Philos. Trans. R. Soc. Lond. B Biol. Sci. *377*, 20200444. https://doi.org/10.1098/rstb.2020.0444.
17. Franklin, T.B., Silva, B.A., Perova, Z., Marrone, L., Masferrer, M.E., Zhan, Y., Kaplan, A., Greetham, L., Verrechia, V., Halman, A., et al. (2017). Prefrontal cortical control of a brainstem social behavior circuit. Nat. Neurosci. *20*, 260–270. https://doi.org/10.1038/nn.4470.
18. Nelson, A.C., Kapoor, V., Vaughn, E., Gnanasegaram, J.A., Rubinstein, N.D., Murthy, V.N., and Dulac, C. (2019). Molecular and circuit architecture of social hierarchy. Preprint at bioRxiv. https://doi.org/10.1101/838664.
19. Goldman-Rakic, P.S. (1996). The prefrontal landscape: implications of functional architecture for understanding human mentation and the central executive. Philos. Trans. R. Soc. Lond. B Biol. Sci. *351*, 1445–1453. https://doi.org/10.1098/rstb.1996.0129.
20. Vertes, R.P. (2004). Differential projections of the infralimbic and prelimbic cortex in the rat. Synapse *51*, 32–58. https://doi.org/10.1002/syn.10279.
21. Gabbott, P.L.A., Warner, T.A., Jays, P.R.L., Salway, P., and Busby, S.J. (2005). Prefrontal cortex in the rat: projections to subcortical autonomic, motor, and limbic centers. J. Comp. Neurol. *492*, 145–177. https://doi.org/10.1002/cne.20738.
22. Anastasiades, P.G., and Carter, A.G. (2021). Circuit organization of the rodent medial prefrontal cortex. Trends Neurosci. *44*, 550–563. https://doi.org/10.1016/j.tins.2021.03.006.
23. Miller, E.K., and Cohen, J.D. (2001). An integrative theory of prefrontal cortex function. Annu. Rev. Neurosci. *24*, 167–202. https://doi.org/10.1146/annurev.neuro.24.1.167.
24. Le Merre, P., Ährlund-Richter, S., and Carlén, M. (2021). The mouse prefrontal cortex: Unity in diversity. Neuron *109*, 1925–1944. https://doi.org/10.1016/j.neuron.2021.03.035.
25. Courtin, J., Chaudun, F., Rozeske, R.R., Karalis, N., Gonzalez-Campo, C., Wurtz, H., Abdi, A., Baufreton, J., Bienvenu, T.C.M., and Herry, C. (2014). Prefrontal parvalbumin interneurons shape neuronal activity to drive fear expression. Nature *505*, 92–96. https://doi.org/10.1038/nature12755.
26. Friedman, A., Homma, D., Gibb, L.G., Amemori, K.I., Rubin, S.J., Hood, A.S., Riad, M.H., and Graybiel, A.M. (2015). A corticostriatal path targeting striosomes controls decision-making under conflict. Cell *161*, 1320–1333. https://doi.org/10.1016/j.cell.2015.04.049.
27. Lui, J.H., Nguyen, N.D., Grutzner, S.M., Darmanis, S., Peixoto, D., Wagner, M.J., Allen, W.E., Kebschull, J.M., Richman, E.B., Ren, J., et al. (2021). Differential encoding in prefrontal cortex projection neuron classes across cognitive tasks. Cell *184*, 489–506.e26. https://doi.org/10.1016/j.cell.2020.11.046.
28. Kim, C.K., Ye, L., Jennings, J.H., Pichamoorthy, N., Tang, D.D., Yoo, A.W., Ramakrishnan, C., and Deisseroth, K. (2017). Molecular and circuit-dynamical identification of top-down neural mechanisms for restraint of reward seeking. Cell *170*, 1013–1027.e14. https://doi.org/10.1016/j.cell.2017.07.020.
29. Otis, J.M., Namboodiri, V.M.K., Matan, A.M., Voets, E.S., Mohorn, E.P., Kosyk, O., McHenry, J.A., Robinson, J.E., Resendez, S.L., Rossi, M.A., and Stuber, G.D. (2017). Prefrontal cortex output circuits guide reward

seeking through divergent cue encoding. Nature *543*, 103–107. https://doi.org/10.1038/nature21376.

30. Warden, M.R., Selimbeyoglu, A., Mirzabekov, J.J., Lo, M., Thompson, K.R., Kim, S.Y., Adhikari, A., Tye, K.M., Frank, L.M., and Deisseroth, K. (2012). A prefrontal cortex-brainstem neuronal projection that controls response to behavioural challenge. Nature *492*, 428–432. https://doi.org/10.1038/nature11617.
31. Land, B.B., Narayanan, N.S., Liu, R.J., Gianessi, C.A., Brayton, C.E., Grimaldi, D.M., Sarhan, M., Guarnieri, D.J., Deisseroth, K., Aghajanian, G.K., and DiLeone, R.J. (2014). Medial prefrontal D1 dopamine neurons control food intake. Nat. Neurosci. *17*, 248–253. https://doi.org/10.1038/nn.3625.
32. Spellman, T., Svei, M., Kaminsky, J., Manzano-Nieves, G., and Liston, C. (2021). Prefrontal deep projection neurons enable cognitive flexibility via persistent feedback monitoring. Cell *184*, 2750–2766.e17. https://doi.org/10.1016/j.cell.2021.03.047.
33. Ko, J. (2017). Neuroanatomical substrates of rodent social behavior: The medial prefrontal cortex and its projection patterns. Front. Neural Circuits *11*, 41. https://doi.org/10.3389/fncir.2017.00041.
34. Huang, W.C., Zucca, A., Levy, J., and Page, D.T. (2020). Social behavior is modulated by valence-encoding mPFC-amygdala sub-circuitry. Cell Rep. *32*, 107899. https://doi.org/10.1016/j.celrep.2020.107899.
35. Jeon, D., Kim, S., Chetana, M., Jo, D., Ruley, H.E., Lin, S.Y., Rabah, D., Kinet, J.P., and Shin, H.S. (2010). Observational fear learning involves affective pain system and Cav1.2 Ca^{2+} channels in ACC. Nat. Neurosci. *13*, 482–488. https://doi.org/10.1038/nn.2504.
36. Scheggia, D., La Greca, F., Maltese, F., Chiacchierini, G., Italia, M., Molent, C., Bernardi, F., Coccia, G., Carrano, N., Zianni, E., et al. (2022). Reciprocal cortico-amygdala connections regulate prosocial and selfish choices in mice. Nat. Neurosci. *25*, 1505–1518. https://doi.org/10.1038/s41593-022-01179-2.
37. Allsop, S.A., Wichmann, R., Mills, F., Burgos-Robles, A., Chang, C.J., Felix-Ortiz, A.C., Vienne, A., Beyeler, A., Izadmehr, E.M., Glober, G., et al. (2018). Corticoamygdala transfer of socially derived information gates observational learning. Cell *173*, 1329–1342.e18. https://doi.org/10.1016/j.cell.2018.04.004.
38. Silverstein, S.E., O'Sullivan, R., Bukalo, O., Pati, D., Schaffer, J.A., Limoges, A., Zsembik, L., Yoshida, T., O'Malley, J.J., Paletzki, R.F., et al. (2024). A distinct cortical code for socially learned threat. Nature *626*, 1066–1072. https://doi.org/10.1038/s41586-023-07008-1.
39. Murugan, M., Jang, H.J., Park, M., Miller, E.M., Cox, J., Taliaferro, J.P., Parker, N.F., Bhave, V., Hur, H., Liang, Y., et al. (2017). Combined social and spatial coding in a descending projection from the prefrontal cortex. Cell *171*, 1663–1677.e16. https://doi.org/10.1016/j.cell.2017.11.002.
40. Choi, T.Y., Jeon, H., Jeong, S., Kim, E.J., Kim, J., Jeong, Y.H., Kang, B., Choi, M., and Koo, J.W. (2024). Distinct prefrontal projection activity and transcriptional state conversely orchestrate social competition and hierarchy. Neuron *112*, 611–627.e8. https://doi.org/10.1016/j.neuron.2023.11.012.
41. Babiczky, Á., and Matyas, F. (2022). Molecular characteristics and laminar distribution of prefrontal neurons projecting to the mesolimbic system. Elife *11*, e78813. https://doi.org/10.7554/eLife.78813.
42. Bloodgood, D.W., Sugam, J.A., Holmes, A., and Kash, T.L. (2018). Fear extinction requires infralimbic cortex projections to the basolateral amygdala. Transl. Psychiatry *8*, 60. https://doi.org/10.1038/s41398-018-0106-x.
43. Liu, W.Z., Wang, C.Y., Wang, Y., Cai, M.T., Zhong, W.X., Liu, T., Wang, Z.H., Pan, H.Q., Zhang, W.H., and Pan, B.X. (2023). Circuit- and laminar-specific regulation of medial prefrontal neurons by chronic stress. Cell Biosci. *13*, 90. https://doi.org/10.1186/s13578-023-01050-2.
44. Gradinaru, V., Thompson, K.R., and Deisseroth, K. (2008). eNpHR: a Natronomonas halorhodopsin enhanced for optogenetic applications. Brain Cell Biol. *36*, 129–139.
45. Shrestha, P., Mousa, A., and Heintz, N. (2015). Layer 2/3 pyramidal cells in the medial prefrontal cortex moderate stress induced depressive behaviors. Elife *4*, e08752. https://doi.org/10.7554/eLife.08752.
46. Zhang, C., Zhu, H., Ni, Z., Xin, Q., Zhou, T., Wu, R., Gao, G., Gao, Z., Ma, H., Li, H., et al. (2022). Dynamics of a disinhibitory prefrontal microcircuit in controlling social competition. Neuron *110*, 516–531.e6. https://doi.org/10.1016/j.neuron.2021.10.034.
47. Gross, C.T., and Canteras, N.S. (2012). The many paths to fear. Nat. Rev. Neurosci. *13*, 651–658. https://doi.org/10.1038/nrn3301.
48. Janak, P.H., and Tye, K.M. (2015). From circuits to behaviour in the amygdala. Nature *517*, 284–292. https://doi.org/10.1038/nature14188.
49. Hoover, W.B., and Vertes, R.P. (2007). Anatomical analysis of afferent projections to the medial prefrontal cortex in the rat. Brain Struct. Funct. *212*, 149–179. https://doi.org/10.1007/s00429-007-0150-4.
50. Likhtik, E., Stujenske, J.M., Topiwala, M.A., Harris, A.Z., and Gordon, J.A. (2014). Prefrontal entrainment of amygdala activity signals safety in learned fear and innate anxiety. Nat. Neurosci. *17*, 106–113. https://doi.org/10.1038/nn.3582.
51. Vialou, V., Bagot, R.C., Cahill, M.E., Ferguson, D., Robison, A.J., Dietz, D.M., Fallon, B., Mazei-Robison, M., Ku, S.M., Harrigan, E., et al. (2014). Prefrontal cortical circuit for depression- and anxiety-related behaviors mediated by cholecystokinin: role of ΔFosB. J. Neurosci. *34*, 3878–3887. https://doi.org/10.1523/JNEUROSCI.1787-13.2014.
52. St Onge, J.R., Stopper, C.M., Zahm, D.S., and Floresco, S.B. (2012). Separate prefrontal-subcortical circuits mediate different components of risk-based decision making. J. Neurosci. *32*, 2886–2899. https://doi.org/10.1523/JNEUROSCI.5625-11.2012.
53. Munuera, J., Rigotti, M., and Salzman, C.D. (2018). Shared neural coding for social hierarchy and reward value in primate amygdala. Nat. Neurosci. *21*, 415–423. https://doi.org/10.1038/s41593-018-0082-8.
54. Kumaran, D., Melo, H.L., and Duzel, E. (2012). The emergence and representation of knowledge about social and nonsocial hierarchies. Neuron *76*, 653–666. https://doi.org/10.1016/j.neuron.2012.09.035.
55. Kim, J., Pignatelli, M., Xu, S., Itohara, S., and Tonegawa, S. (2016). Antagonistic negative and positive neurons of the basolateral amygdala. Nat. Neurosci. *19*, 1636–1646. https://doi.org/10.1038/nn.4414.
56. Piantadosi, S.C., Zhou, Z.C., Pizzano, C., Pedersen, C.E., Nguyen, T.K., Thai, S., Stuber, G.D., and Bruchas, M.R. (2024). Holographic stimulation of opposing amygdala ensembles bidirectionally modulates valence-specific behavior via mutual inhibition. Neuron *112*, 593–610.e5. https://doi.org/10.1016/j.neuron.2023.11.007.
57. Rosvold, H.E., Mirsky, A.F., and Pribram, K.H. (1954). Influence of amygdalectomy on social behavior in monkeys. J. Comp. Physiol. Psychol. *47*, 173–178. https://doi.org/10.1037/h0058870.
58. Emery, N.J., Capitanio, J.P., Mason, W.A., Machado, C.J., Mendoza, S.P., and Amaral, D.G. (2001). The effects of bilateral lesions of the amygdala on dyadic social interactions in rhesus monkeys (Macaca mulatta). Behav. Neurosci. *115*, 515–544. https://doi.org/10.1037//0735.115.3.515.
59. Machado, C.J., and Bachevalier, J. (2006). The impact of selective amygdala, orbital frontal cortex, or hippocampal formation lesions on established social relationships in rhesus monkeys (Macaca mulatta). Behav. Neurosci. *120*, 761–786. https://doi.org/10.1037/0735-7044.120.4.761.
60. Edwards, D.H., and Kravitz, E.A. (1997). Serotonin, social status and aggression. Curr. Opin. Neurobiol. *7*, 812–819. https://doi.org/10.1016/s0959-4388(97)80140-7.
61. Raleigh, M.J., McGuire, M.T., Brammer, G.L., Pollack, D.B., and Yuwiler, A. (1991). Serotonergic mechanisms promote dominance acquisition in adult male vervet monkeys. Brain Res. *559*, 181–190. https://doi.org/10.1016/0006-8993(91)90001-c.
62. Audero, E., Mlinar, B., Baccini, G., Skachokova, Z.K., Corradetti, R., and Gross, C. (2013). Suppression of serotonin neuron firing increases

aggression in mice. J. Neurosci. *33*, 8678–8688. https://doi.org/10.1523/JNEUROSCI.2067-12.2013.

63. Caramaschi, D., de Boer, S.F., and Koolhaas, J.M. (2007). Differential role of the 5-HT1A receptor in aggressive and non-aggressive mice: an across-strain comparison. Physiol. Behav. *90*, 590–601. https://doi.org/10.1016/j.physbeh.2006.11.010.

64. Amat, J., Baratta, M.V., Paul, E., Bland, S.T., Watkins, L.R., and Maier, S.F. (2005). Medial prefrontal cortex determines how stressor controllability affects behavior and dorsal raphe nucleus. Nat. Neurosci. *8*, 365–371. https://doi.org/10.1038/nn1399.

65. Amat, J., Paul, E., Zarza, C., Watkins, L.R., and Maier, S.F. (2006). Previous experience with behavioral control over stress blocks the behavioral and dorsal raphe nucleus activating effects of later uncontrollable stress: Role of the ventral medial prefrontal cortex. J. Neurosci. *26*, 13264–13272. https://doi.org/10.1523/Jneurosci.3630-06.2006.

66. Calizo, L.H., Akanwa, A., Ma, X., Pan, Y.Z., Lemos, J.C., Craige, C., Heemstra, L.A., and Beck, S.G. (2011). Raphe serotonin neurons are not homogenous: electrophysiological, morphological and neurochemical evidence. Neuropharmacology *61*, 524–543. https://doi.org/10.1016/j.neuropharm.2011.04.008.

67. Weissbourd, B., Ren, J., DeLoach, K.E., Guenthner, C.J., Miyamichi, K., and Luo, L. (2014). Presynaptic partners of dorsal raphe serotonergic and GABAergic neurons. Neuron *83*, 645–662. https://doi.org/10.1016/j.neuron.2014.06.024.

68. Kirby, L.G., Pernar, L., Valentino, R.J., and Beck, S.G. (2003). Distinguishing characteristics of serotonin and non-serotonin-containing cells in the dorsal raphe nucleus: electrophysiological and immunohistochemical studies. Neuroscience *116*, 669–683. https://doi.org/10.1016/s0306-4522(02)00584-5.

69. Okaty, B.W., Freret, M.E., Rood, B.D., Brust, R.D., Hennessy, M.L., deBairos, D., Kim, J.C., Cook, M.N., and Dymecki, S.M. (2015). Multi-scale molecular deconstruction of the serotonin neuron system. Neuron *88*, 774–791. https://doi.org/10.1016/j.neuron.2015.10.007.

70. Adams, D.B. (1968). Cells related to fighting behavior recorded from midbrain central gray neuropil of cat. Science *159*, 894–896. https://doi.org/10.1126/science.159.3817.894.

71. Hunsperger, R.W. (1956). Role of substantia grisea centralis mesencephali in electrically-induced rage reactions. Prog. Neurobiol. *1956*, 289–294.

72. Mos, J., Kruk, M.R., Van Poel, A.M.D., and Meelis, W. (1982). Aggressive behavior induced by electrical stimulation in the midbrain central gray of male rats. Aggr. Behav. *8*, 261–284.

73. Fernandez De Molina, A., and Hunsperger, R.W. (1962). Organization of the subcortical system governing defence and flight reactions in the cat. J. Physiol. *160*, 200–213. https://doi.org/10.1113/jphysiol.1962.sp006841.

74. Mos, J., Lammers, J.H.C.M., van der Poel, A.M., Bermond, B., Meelis, W., and Kruk, M.R. (1983). Effects of midbrain central gray lesions on spontaneous and electrically induced aggression in the rat. Aggr. Behav. *9*, 133–155.

75. Carrive, P. (1993). The periaqueductal gray and defensive behavior: functional representation and neuronal organization. Behav. Brain Res. *58*, 27–47. https://doi.org/10.1016/0166-4328(93)90088-8.

76. Bandler, R., and Shipley, M.T. (1994). Columnar organization in the midbrain periaqueductal gray: modules for emotional expression? Trends Neurosci. *17*, 379–389. https://doi.org/10.1016/0166-2236(94)90047-7.

77. Tovote, P., Esposito, M.S., Botta, P., Chaudun, F., Fadok, J.P., Markovic, M., Wolff, S.B.E., Ramakrishnan, C., Fenno, L., Deisseroth, K., et al. (2016). Midbrain circuits for defensive behaviour. Nature *534*, 206–212. https://doi.org/10.1038/nature17996.

78. Evans, D.A., Stempel, A.V., Vale, R., Ruehle, S., Lefler, Y., and Branco, T. (2018). A synaptic threshold mechanism for computing escape decisions. Nature *558*, 590–594. https://doi.org/10.1038/s41586-018-0244-6.

79. Falkner, A.L., Wei, D.Y., Song, A., Watsek, L.W., Chen, I., Chen, P., Feng, J.E., and Lin, D.Y. (2020). Hierarchical representations of aggression in a hypothalamic-midbrain circuit. Neuron *106*, 637–648.e6. https://doi.org/10.1016/j.neuron.2020.02.014.

80. Keay, K.A., and Bandler, R. (2001). Parallel circuits mediating distinct emotional coping reactions to different types of stress. Neurosci. Biobehav. Rev. *25*, 669–678. https://doi.org/10.1016/S0149-7634(01)00049-5.

81. Vander Weele, C.M., Siciliano, C.A., Matthews, G.A., Namburi, P., Izadmehr, E.M., Espinel, I.C., Nieh, E.H., Schut, E.H.S., Padilla-Coreano, N., Burgos-Robles, A., et al. (2018). Dopamine enhances signal-to-noise ratio in cortical-brainstem encoding of aversive stimuli. Nature *563*, 397–401. https://doi.org/10.1038/s41586-018-0682-1.

82. Larrieu, T., Cherix, A., Duque, A., Rodrigues, J., Lei, H., Gruetter, R., and Sandi, C. (2017). Hierarchical status predicts behavioral vulnerability and nucleus accumbens metabolic profile following chronic social defeat stress. Curr. Biol. *27*, 2202–2210.e4. https://doi.org/10.1016/j.cub.2017.06.027.

83. Hollis, F., van der Kooij, M.A., Zanoletti, O., Lozano, L., Cantó, C., and Sandi, C. (2015). Mitochondrial function in the brain links anxiety with social subordination. Proc. Natl. Acad. Sci. USA *112*, 15486–15491. https://doi.org/10.1073/pnas.1512653112.

84. van der Kooij, M.A., Hollis, F., Lozano, L., Zalachoras, I., Abad, S., Zanoletti, O., Grosse, J., Guillot de Suduiraut, I., Canto, C., and Sandi, C. (2018). Diazepam actions in the VTA enhance social dominance and mitochondrial function in the nucleus accumbens by activation of dopamine D1 receptors. Mol. Psychiatry *23*, 569–578. https://doi.org/10.1038/mp.2017.135.

85. de Jong, J.W., Fraser, K.M., and Lammel, S. (2022). Mesoaccumbal dopamine heterogeneity: What do dopamine firing and release have to do with it? Annu. Rev. Neurosci. *45*, 109–129. https://doi.org/10.1146/annurev-neuro-110920-011929.

86. Floresco, S.B. (2015). The nucleus accumbens: an interface between cognition, emotion, and action. Annu. Rev. Psychol. *66*, 25–52. https://doi.org/10.1146/annurev-psych-010213-115159.

87. Shan, Q., Hu, Y., Chen, S., and Tian, Y. (2022). Nucleus accumbens dichotomically controls social dominance in male mice. Neuropsychopharmacology *47*, 776–787. https://doi.org/10.1038/s41386-021-01220-1.

88. Bault, N., Joffily, M., Rustichini, A., and Coricelli, G. (2011). Medial prefrontal cortex and striatum mediate the influence of social comparison on the decision process. Proc. Natl. Acad. Sci. USA *108*, 16044–16049. https://doi.org/10.1073/pnas.1100892108.

89. Noh, K., Cho, W.H., Lee, B.H., Kim, D.W., Kim, Y.S., Park, K., Hwang, M., Barcelon, E., Cho, Y.K., Lee, C.J., et al. (2023). Cortical astrocytes modulate dominance behavior in male mice by regulating synaptic excitatory and inhibitory balance. Nat. Neurosci. *26*, 1541–1554. https://doi.org/10.1038/s41593-023-01406-4.

90. Tada, H., Miyazaki, T., Takemoto, K., Takase, K., Jitsuki, S., Nakajima, W., Koide, M., Yamamoto, N., Komiya, K., Suyama, K., et al. (2016). Neonatal isolation augments social dominance by altering actin dynamics in the medial prefrontal cortex. Proc. Natl. Acad. Sci. USA *113*, E7097–E7105. https://doi.org/10.1073/pnas.1606351113.

91. Gilbert, C.D., and Wiesel, T.N. (1983). Functional organization of the visual cortex. Prog. Brain Res. *58*, 209–218. https://doi.org/10.1016/S0079-6123(08)60022-9.

92. Manoocheri, K., and Carter, A.G. (2022). Rostral and caudal basolateral amygdala engage distinct circuits in the prelimbic and infralimbic prefrontal cortex. Elife *11*, e82688. https://doi.org/10.7554/eLife.82688.

93. Pouille, F., Marin-Burgin, A., Adesnik, H., Atallah, B.V., and Scanziani, M. (2009). Input normalization by global feedforward inhibition expands cortical dynamic range. Nat. Neurosci. *12*, 1577–1585. https://doi.org/10.1038/nn.2441.

94. DeNardo, L.A., Berns, D.S., DeLoach, K., and Luo, L.Q. (2015). Connectivity of mouse somatosensory and prefrontal cortex examined with trans-synaptic tracing. Nat. Neurosci. *18*, 1687–1697. https://doi.org/10.1038/nn.4131.

95. Friard, O.G., and Gamba, M. (2016). BORIS: a free, versatile open-source event-logging software for video/audio coding and live observations. Methods Ecol. Evol. *7*, 1325–1330.

96. Fan, Z., Zhu, H., Zhou, T., Wang, S., Wu, Y., and Hu, H. (2019). Using the tube test to measure social hierarchy in mice. Nat. Protoc. *14*, 819–831. https://doi.org/10.1038/s41596-018-0116-4.

97. Li, Y., Zhong, W., Wang, D., Feng, Q., Liu, Z., Zhou, J., Jia, C., Hu, F., Zeng, J., Guo, Q., et al. (2016). Serotonin neurons in the dorsal raphe nucleus encode reward signals. Nat. Commun. *7*, 10503. https://doi.org/10.1038/ncomms10503.

Please cite this article in press as: Xin et al., Deconstructing the neural circuit underlying social hierarchy in mice, Neuron (2024), https://doi.org/10.1016/j.neuron.2024.11.007

STAR★METHODS

KEY RESOURCES TABLE

REAGENT or RESOURCE	SOURCE	IDENTIFIER
Antibodies		
Goat anti-rabbit IgG Alexa Fluor 488	Thermo Fisher Scientific	Cat# A-11034; RRID:AB_2576217
Rabbit anti-c-Fos	Synaptic Systems	Cat# 226008; RRID:AB_2891278
Bacterial and virus strains		
AAV2/9-hSyn-eNpHR3.0-mCherry-WPRE-pA	Taitool Bioscience, Shanghai	Cat# S0463-9
AAV2/9-CAG-hChR2 (H134R)-tdTomato	Taitool Bioscience, Shanghai	Cat# S0168-9
AAV2/9-hSyn-HA-hM4D-IRES-mCitrine	Umass	N/A
AAV2/9-hSyn-hM4D(Gi)-mCherry-WPRE-pA	Taitool Bioscience, Shanghai	Cat# S0488-9-h50
AAV2/9-hSyn-mCherry-WPRE-pA	Taitool Bioscience, Shanghai	Cat# S0238-9
AAV2/2Retro-hSyn-Cre-WPRE-pA	Taitool Bioscience, Shanghai	Cat# S0278-2R
AAV2/9-CAG-Flex-GCaMP6s-WPRE-pA	Taitool Bioscience, Shanghai	Cat# S0354-9
AAV2/9-hEF1a-DIO-EYFP-WPRE-pA	Taitool Bioscience, Shanghai	Cat# S0196-9-H50
pAAV2/9-EF1a-DIO-eNpHR3.0-mCherry	OBIO Technology, Shanghai	Cat# H4882
AAV2/9-EF1a-DIO-hChR2(H134R)-ER2-P2A-EGFP	Taitool Bioscience, Shanghai	Cat# S0724-9-H50
AAV2/2RetroPlus-hSyn-tdTomato-WPRE-pA	Taitool Bioscience, Shanghai	Cat# S0266-2RP-H20
AAV2/8-hSyn-Synaptophysin-mRuby-T2A-H2B-EGFP	Taitool Bioscience, Shanghai	Cat# S0250-9-H20
rAAV2/9-nEF1α-FDIO-hChR2(H134R)-EYFP	Brain Case, Shenzhen	Cat# BC-0112
AAV2/2Retro-hSyn-Flpo-WPRE-pA	Taitool Bioscience, Shanghai	Cat# S0271-2R
Chemicals, peptides, and recombinant proteins		
Pentobarbital sodium	Sigma	Cat# P3761
CTB-488	Thermo Fisher Scientific	C34775
CTB-555	Thermo Fisher Scientific	C34776
CTB-647	Thermo Fisher Scientific	C34778
Tetrodotoxin citrate (TTX)	alomone labs	T-550-1 mg
4-Aminopyridine (4AP)	Tocris	0940-100 mg
Picrotoxin (PTX)	Tocris	1128-1 g
Experimental models: Organisms/strains		
Mouse: C57BL/6J	SLAC or Jihui Laboratory animal, Shanghai	N/A
Mouse: Thy1-ChR2-YFP	The Jackson Laboratory	JAX.007615; RRID:IMSR_JAX:007615
Mouse: Wfs1-Tg2-CreERT2	The Jackson Laboratory	JAX.009614; RRID:IMSR_JAX:009614
Software and algorithms		
OmniPlex neural recording data acquisition system	Plexon	https://plexon.com/products/omniplex-software
NeuroExplorer	Plexon	https://plexon.com/products/neuroexplorer
Offline Sorter	Plexon	https://plexon.com/products/offline-sorter
pCLAMP10 software	Molecular Devices	https://www.moleculardevices.com/products/axon-patch-clamp-system
MultiClamp 700B amplifier	Molecular Devices	https://www.moleculardevices.com/products/axon-patch-clamp-system
DigiData 1550 digitizer	Molecular Devices	https://www.moleculardevices.com/products/axon-patch-clamp-system

(*Continued on next page*)

Please cite this article in press as: Xin et al., Deconstructing the neural circuit underlying social hierarchy in mice, Neuron (2024), https://doi.org/10.1016/j.neuron.2024.11.007

Continued

REAGENT or RESOURCE	SOURCE	IDENTIFIER
MATLAB R2021a	MathWorks	https://www.mathworks.com/products/matlab.html
Prism 7.0	GraphPad Software	https://www.graphpad.com/scientific-software/prism
BORIS	Friard and Gamba[95]	http://www.boris.unito.it/
CamFibrePhotometry	ThinkerTech, Nanjing	http://www.thinkerbiotech.com/
ImageJ	National Institutes of Health	https://imagej.nih.gov/ij/index.html
Analysis code	Zhang et al.[46]	https://zenodo.org/record/5591050
Other		
473-nm and 589-nm laser LED	Inper, China	https://www.inper.com
Fiber photometry system	ThinkerTech, Nanjing	http://www.thinkerbiotech.com/

EXPERIMENTAL MODEL AND STUDY PARTICIPANT DETAILS

Animals

Male adult (over 8 weeks of age) C57BL/6J strain mice (SLAC or Jihui Laboratory animal, Shanghai), Thy1-ChR2-YFP (The Jackson Laboratory, JAX.007615) and Wfs1-Tg2-CreERT2 (The Jackson Laboratory, JAX.009614) transgenetic mice were used for experiments. Mice were housed in groups of 4 randomly under standard conditions (12-h light/dark cycle with food and water available *ad libitum*). All animal studies and experimental procedures were conducted in accordance with the guidelines of the Animal Care and Use Committee of the animal facility at Zhejiang University.

METHOD DETAILS

Tube test

The tube test assay was performed as previously described.[96] A transparent tube of 30-cm length and 3-cm inside diameter was used to allow a single mouse to pass through. To enable mice wearing optic fibers to go through the tube, a 12-mm slit was made at the top of the tube. On the first day of training, each mouse was trained to pass through the tube in alternating directions for 10 trials per day. Subsequently, each mouse was trained to push an object of its own weight for 10 trials per day for 2 consecutive days. After training, mice were tested in pairs. Each pair of mice was simultaneously released from opposite ends of the tube. When the mice met in the middle of the tube, the mouse that first retreated with four paws out of the tube was designated as the "loser", and the other mouse was designated as the "winner". The rank of each mouse was determined by the total number of wins on each test day. Only mice cages with stable ranks (all mice maintained at the same rank position for over 4 consecutive days) were used for further optogenetic and chemogenetic manipulations.

Using frame-to-frame video annotation, we unambiguously identified three types of behaviors during each tube test competition: push (one mouse shoves its head under another mouse), resistance (holding onto the territory when being pushed, often with the head being pushed up), and retreat (backing out after being pushed or voluntarily withdrawing, often characterized by bending down of head). These behavior epochs were manually annotated and marked using the BORIS software.[95]

c-Fos immunohistochemistry staining

Mice were habituated to the tube for 3 days, during which they were trained to pass through the tube in alternating directions 10 times per day. On the test day, after habituation in the experimental environment, two cagemate mice were simultaneously released from the opposite ends and met in the middle of the tube. Winner and loser mice were then determined. To enhance c-Fos expression signals, the tube test was repeated for 6 times between the same pair of winner and loser mice. Only mice pairs that consistently showed the same competition outcomes were used for subsequent experiments. Other mice from the same cage were used as controls and allowed to pass through the tube 6 times without encountering another mouse. After the tube tests, mice were monitored for 2 h to ensure that there were no fights within the group. Two hours after the last tube test, mice were deeply anesthetized with 1% sodium pentobarbital (100 mg/kg body weight) and perfused transcardially with 50 mL of 0.1 M phosphate-buffered saline (PBS) followed by 50 mL of 4% w/v paraformaldehyde (PFA) in PBS. Brains were removed and postfixed overnight in the same fixative and cryoprotected in 30% w/v sucrose in PBS. Coronal brain sections (40 μm) were serially cut using a cryostat (CM1950, Leica) and divided into 3 interleaved sets.

Staining for c-Fos was performed using Rabbit anti-c-Fos as the primary antibody (1:5000; Synaptic Systems) and Goat anti-rabbit IgG Alexa Fluor 488 as the secondary antibody (1:1000, Thermo Fisher Scientific). The slices were then counterstained with DAPI or Hoechst before imaging with an Olympus VS120 virtual microscopy slide scanning system. Investigators counted c-Fos-positive cells blindly with respect to the assignment of mice groups. The number of c-Fos-positive cells of each brain region is the average

of one interleaved set of brain slices. The c-Fos-positive cell number was normalized to the average c-Fos-positive cell number of the control group for each subject.

Stereotactic surgeries

After being anaesthetized with 1% sodium pentobarbital (100 mg/kg body weight), mice were head-fixed in a stereotaxic frame (RWD Instruments). A glass pipette with a pressure microinjector (Picospritzer III, Parker) was used to deliver virus (0.2 μl per site) or neural tracer (0.3 μl per site) to target brain regions.

For the inhibition of dmPFC downstream pathways, AAV2/9-hSyn-eNpHR3.0-mCherry-WPRE-pA (titre: 1.76 × 10^{13} v.g./ml, dilution: 1:5, Taitool Bioscience) or control virus AAV2/9-hSyn-mCherry-WPRE-pA (titre: 2.49 × 10^{13} v.g./ml, dilution: 1:8, Taitool Bioscience) was bilaterally injected into the dmPFC (AP: + 2.43 mm from bregma, ML: ± 0.4 mm from midline, DV: - 1.2 mm from dura), and dual fiber-optic cannulae (NA = 0.37, Newdoon or Inper) were implanted into its downstream brain regions including the aBLA (AP: - 1.5 mm from bregma, ML: ± 3.28 mm from midline, DV: - 3.5 mm from dura), DRN (AP: 0 mm from lamda, ML: ± 1.0 mm from midline, DV: - 2.7 mm from skull surface) at a 20° angle in the ML direction, PAG (AP: - 4.15 mm from bregma, ML: ± 1.2 mm from midline, DV: - 1.8 mm from dura) at a 20° angle in the ML direction, MDT (AP: -1.5 mm from bregma, ML: ± 0.4 mm from midline, DV: - 2.95 mm from dura), dmCPu (AP: + 1.1 mm from bregma, ML: ± 1.2 mm from midline, DV: - 1.9 mm from dura) and NAc (AP: + 1.1 mm from bregma, ML: ± 1.2 mm from midline, DV: - 3.25 mm from dura).

For the activation of dmPFC downstream pathways, AAV2/9-CAG-hChR2 (H134R)-tdTomato (titre: 1.32 × 10^{13} v.g./ml, dilution: 1:5, Taitool Bioscience) or control virus AAV2/9-hSyn-mCherry-WPRE-pA (titre: 2.49 × 10^{13} v.g./ml, dilution: 1:8, Taitool Bioscience) was injected into the right dmPFC (AP: + 2.43 mm from bregma, ML: + 0.4 mm from midline, DV: - 1.2 mm from dura), and a mono fiber-optic cannula was implanted into the right aBLA (AP: - 1.5 mm from bregma, ML: + 3.28 mm from midline, DV: - 3.5 mm from dura), DRN (AP: 0 mm from lamda, ML: + 1.0 mm from midline, DV: - 2.7 mm from skull surface) at a 20° angle in the ML direction, and PAG (AP: - 4.15 mm from bregma, ML: + 1.2 mm from midline, DV: - 1.8 mm from dura) at a 20° angle in the ML direction.

For the activation of DRN, PAG and aBLA-projecting neurons in the dmPFC, AAV2/2Retro-hSyn-Cre-WPRE-pA (titre: 1.82 × 10^{13} v.g./ml, dilution: 1:2, Taitool Bioscience) was injected into the right DRN (AP: 0 mm from lamda, ML: + 1.0 mm from midline, DV: - 3.0 mm from skull surface) at a 20° angle in the ML direction, PAG (AP: - 4.15 mm from bregma, ML: + 1.2 mm from midline, DV: - 2.1 mm from dura) at a 20° angle in the ML direction, and aBLA (AP: -1.5 mm from bregma, ML: + 3.28 mm from midline, DV: -3.8 mm from dura), respectively. AAV2/9-EF1a-DIO-hChR2(H134R)-ER2-P2A-EGFP (titre: 1.14 × 10^{13} v.g./ml, dilution: 1:5, Taitool Bioscience) was injected into the right dmPFC (AP: + 2.43 mm from bregma, ML: + 0.2 mm (for aBLA) or + 0.4 mm (for DRN and PAG) from midline, DV: -1.2 mm from dura). A mono fiber-optic cannula was implanted 300 - 400 μm above the viral injection coordinates within the dmPFC.

For the optogenetic inhibition of the aBLA, AAV2/9-hSyn-eNpHR3.0-mCherry-WPRE-pA (titre: 1.76 × 10^{13} v.g./ml, dilution: 1:5, Taitool Bioscience) or control virus AAV2/9-hSyn-mCherry-WPRE-pA (titre: 2.49 × 10^{13} v.g./ml, dilution: 1:8, Taitool Bioscience) was bilaterally injected into the aBLA (AP: - 1.5 mm from bregma, ML: + 3.28 mm from midline, DV: - 3.8 mm from dura), and dual fiber-optic cannulae was implanted 300 - 400 μm above the viral injection coordinates. For the optogenetic stimulation of the aBLA, AAV2/9-CAG-hChR2 (H134R)-tdTomato (titre: 1.32 × 10^{13} v.g./ml, dilution: 1:5, Taitool Bioscience) or control virus AAV2/9-hSyn-mCherry-WPRE-pA (titre: 2.49 × 10^{13} v.g./ml, dilution: 1:8, Taitool Bioscience) was injected into the right aBLA (AP: - 1.5 mm from bregma, ML: + 3.28 mm from midline, DV: - 3.8 mm from dura), and a mono fiber-optic cannula was implanted 300 - 400 μm above the viral injection coordinates.

For the chemogenetic inhibition of the aBLA, AAV virus encoding Cre-dependent inhibitory DREADD, the engineered Gi-coupled hM4D receptor (AAV2/9-hSyn-HA-hM4D-IRES-mCitrine; titre: 1.8 × 10^{13} v.g./ml, dilution: 1:5, Umass; or AAV2/9-hSyn-hM4D(Gi)-mCherry-WPRE-pA; titre: 2.66 × 10^{13} v.g./ml, dilution: 1:10, Taitool Bioscience) or control virus AAV2/9-hSyn-mCherry-WPRE-pA (titre: 2.49 × 10^{13} v.g./ml, dilution: 1:8, Taitool Bioscience) was injected bilaterally into the aBLA (AP: - 1.5 mm from bregma, ML: ± 3.28 mm from midline, DV: - 3.8 mm from dura). For the chemogenetic inhibition of the pBLA, AAV2/9-hSyn-hM4D(Gi)-mCherry-WPRE-pA (titre: 2.66 × 10^{13} v.g./ml, dilution: 1:10, Taitool Bioscience) was injected bilaterally into the pBLA (AP: - 2.0 mm from bregma, ML: ± 3.35 mm from midline, DV: - 4.0 mm from dura).

For the activation of layer 2/3-specific neurons in the dmPFC, AAV2/9-EF1a-DIO-hChR2(H134R)-ER2-P2A-EGFP (titre: 1.14 × 10^{13} v.g./ml, dilution: 1:5, Taitool Bioscience) was injected into the right dmPFC (AP: + 2.43 mm from bregma, ML: + 0.2 mm from midline, DV: - 1.2 mm from dura) of Wfs1-Tg2-CreERT2 mice. A mono fiber-optic cannula was implanted 300 - 400 μm above the viral injection coordinates with a 15° angle in the ML direction. For activation of layer 5-specific neurons in the dmPFC, a mono fiber-optic cannula was implanted in the right dmPFC (AP: + 2.43 mm from bregma, ML: + 0.4 mm from midline, DV: - 0.8 mm from dura) of Thy1-ChR2-YFP mice.

For anterograde tracing experiments, AAV2/8-hSyn-Synaptophysin-mRuby-T2A-H2B-EGFP (titre: 3.88 × 10^{12} v.g./ml, no dilution, Taitool Bioscience) was injected into the right dmPFC (AP: + 2.43 mm from bregma, ML: + 0.4 mm from midline, DV: - 1.2 mm from dura). For the retrograde tracing experiments, 0.3 μl of cholera toxin b subunit conjugated to fluorophores (CTB-488, CTB-555, CTB-647, 2 ug/ul, Invitrogen, Thermo Fisher Scientific) was unilaterally injected into the right aBLA (AP: - 1.5 mm from bregma, ML: + 3.28 mm from midline, DV: - 3.8 mm from dura), DRN (AP: 0 mm from lamda, ML: + 1.0 mm from midline, DV: - 3.0 mm from skull surface) at a 20° angle in the ML direction and PAG (AP: - 4.15 mm from bregma, ML: + 1.2 mm from midline, DV: - 2.1 mm from dura) at a 20° angle in the ML direction, respectively.

For fiber photometry experiments, AAV2/2Retro-hSyn-Cre-WPRE-pA (titre: 1.82 × 10^{13} v.g./ml, dilution: 1:2, Taitool Bioscience) was injected into the right aBLA (AP: - 1.5 mm from bregam, ML: + 3.28 mm from midline, DV: - 3.8 mm from dura), DRN (AP: 0 mm from lamda, ML: + 1.0 mm from midline, DV: - 3.0 mm from skull surface) at a 20° angle in the ML direction or PAG (AP: - 4.15 mm from bregma, ML: + 1.2 mm from midline, DV: - 2.1 mm from dura) at a 20° angle in the ML direction. AAV2/9-CAG-Flex-GCaMP6s-WPRE-pA (1.69 × 10^{13} v.g./ml, dilution: 1: 10, Taitool Bioscience) or control virus AAV2/9-hEF1a-DIO-EYFP-WPRE-pA (1.3 × 10^{13} v.g./ml, dilution: 1: 10, Taitool Bioscience) was injected into the dmPFC (AP: + 2.43 mm from bregma, ML: + 0.2 mm (for aBLA) or + 0.4 mm (for DRN and PAG) from midline, DV: - 1.2 mm from dura) to express the calcium indicator GCaMP6s in dmPFC projection neurons. A mono fiber-optic cannula was implanted 200 μm above viral injection coordinates within the dmPFC.

For *in vivo* recording experiments, to optogenetically activate or inhibit aBLA-projecting dmPFC neurons. AAV2/2Retro-hSyn-Cre-WPRE-pA (titre: 1.82 × 10^{13} v.g./ml, dilution: 1:2, Taitool Bioscience) was injected into the right aBLA (AP: - 1.5 mm from bregma, ML: + 3.28 mm from midline, DV: - 3.8 mm from dura). Then, AAV2/9-EF1a-DIO-hChR2(H134R)-ER2-P2A-EGFP (titre: 1.14 × 10^{13} v.g./ml, dilution: 1:5, Taitool Bioscience) or pAAV2/9-Ef1a–DIO-eNpHR3.0-mCherry (titre: 5.89 × 10^{12} v.g./ml, dilution: 1:2, OBIO Technology) was injected into the right dmPFC (AP: + 2.43 mm from bregma, ML: + 0.2 mm from midline, DV: - 1.2 mm from dura) to specifically express ChR2 or eNpHR3.0 in aBLA-projecting neurons in the dmPFC. To optogenetically activate or inhibit DRN-projecting dmPFC neurons. AAV2/2Retro-hSyn-Cre-WPRE-pA (titre: 1.82 × 10^{13} v.g./ml, dilution: 1:2, Taitool Bioscience) was injected into the right DRN (AP: 0 mm from lamda, ML: + 1.0 mm from midline, DV: - 3.0 mm from skull surface) at a 20° angle in the ML direction. Then, AAV2/9-EF1a-DIO-hChR2(H134R)-ER2-P2A-EGFP (titre: 1.14 × 10^{13} v.g./ml, dilution: 1:5, Taitool Bioscience) or pAAV2/9-Ef1a-DIO-eNpHR3.0-mCherry (titre: 5.89 × 10^{12} v.g./ml, dilution: 1:2, OBIO Technology) was injected into the right dmPFC (AP: + 2.43 mm from bregma, ML: + 0.4 mm from midline, DV: - 1.2 mm from dura) to specifically express ChR2 or eNpHR3.0 in DRN-projecting dmPFC neurons.

For *in vitro* recording experiments, AAV2/2Retro-hSyn-Cre-WPRE-pA (titre: 1.82 × 10^{13} v.g./ml, dilution: 1:2, Taitool Bioscience) was injected into the right aBLA (AP: - 1.5 mm from bregma, ML: + 3.28 mm from midline, DV: - 3.8 mm from dura) to optogenetically stimulate aBLA-projecting neurons in the dmPFC. Then, AAV2/9-EF1a-DIO-hChR2(H134R)-ER2-P2A-EGFP (titre: 1.14 × 10^{13} v.g./ml, dilution: 1:5, Taitool Bioscience) was injected into the right dmPFC (AP: + 2.43 mm from bregma, ML: + 0.2 mm from midline, DV: - 1.2 mm from dura) to specifically express ChR2 in aBLA-projecting neurons in the dmPFC. To visualize DRN-projecting dmPFC neurons, AAV2/2RetroPlus-hSyn-tdTomato-WPRE-pA (titre: 1.06 × 10^{13} v.g./ml, dilution: 1:2, Taitool Bioscience) was injected in the right DRN (AP: 0 mm from lamda, ML: + 1.0 mm from midline, DV: - 3.0 mm from skull surface) at a 20° angle in the ML direction to label DRN-projecting neurons in the dmPFC. For *in vitro* recording experiments using PV-Cre or SST-Cre mice, pAAV-Ef1a-DIO-eNpHR3.0-mCherry (titre: 5.89 × 10^{12} v.g./ml, dilution: 1:2, OBIO Technology) was injected into the right dmPFC (AP: + 2.43 mm from bregma, ML: + 0.4 mm from midline, DV: - 1.2 mm from dura) to specifically express eNpHR3.0 in PV or SST neurons, respectively. rAAV2/9-nEF1α-FDIO-hChR2(H134R)-EYFP (titre: 5.51 × 10^{12} v.g./ml, no dilution, Brain Case) was injected into the right dmPFC (AP: + 2.43 mm from bregma, ML: + 0.2 mm from midline, DV: - 1.2 mm from dura), and retrograde virus AAV2/2Retro-hSyn-Flpo-WPRE-pA (titre: 1.94 × 10^{13} v.g./ml, no dilution, Taitool Bioscience) was injected into the right aBLA (AP: - 1.5 mm from bregma, ML: + 3.28 mm from midline, DV: - 3.8 mm from dura) to specifically express ChR2 in aBLA-projecting neurons.

The glass pipette was withdrawn 10 min after injection. Optic fibers were cemented onto the skull using dental acrylic. After surgery, mice were allowed to recover from anesthesia on a heat pad. Mice were transcardially perfused under deep anesthesia with 0.1 M phosphate-buffered saline (PBS) followed by 4% w/v paraformaldehyde (PFA) after all experiments to verify the sites of virus injection and optic fiber location. Brains were collected and postfixed in 4% w/v PFA overnight, followed by cryoprotection with a 30% w/v sucrose solution for 1-2 days. Dehydrated brains were then sectioned into 70 μm thick coronal slices using a cryostat (CM1950, Leica). The slices were then counterstained with DAPI or Hoechst before imaging. Fluorescent image acquisition was performed with an Olympus VS120 virtual microscopy slide scanning system. Only data from mice with correct virus injection site and optic fiber location site were used.

Optogenetic and chemogenetic manipulations in tube test

All optogenetic manipulation experiments were conducted at least 4 weeks after viral injection to allow the full expression of ChR2 or eNpHR3.0. On the test day, subject mice were habituated to fiber connection. Tube test ranks were confirmed again under light-off conditions with other cagemates wearing fake optic fiber connectors. To determine the light frequency for optogenetic activation, we injected AAV2/9-CAG-hChR2 (H134R)-tdTomato into the dmPFC, and recorded light-induced spiking of aBLA neurons in brain slices while photostimulating dmPFC-aBLA terminals with 473-nm blue light under different frequencies including 5 Hz, 10 Hz, 20 Hz and 50 Hz (10 ms pulse width). We found that 5 Hz light stimulation induced a highest fidelity of light-induced spiking in aBLA neurons (Figure S4). Therefore, in optogenetic activation light-on trials, the 473-nm blue light was delivered at 5 Hz, 10 ms pulse right before tube entering and throughout the test. Light intensity was gradually increased until the rank changed or the maximal 30 mW light intensity was reached. In optogenetic inhibition light-on trials, a 589-nm yellow light was delivered constantly before tube entering and throughout the test. Light intensity was gradually increased until the rank changed or the maximal 10 mW light intensity was reached. The light intensity that induced rank change was 3.20 ± 0.53 mW for dmPFC-DRN terminal::eNpHR3.0, 6.70 ± 3.37 mW for dmPFC-DRN terminal::ChR2, 6.14 ± 1.23 mW for dmPFC-PAG terminal::eNpHR3.0, 8.56 ± 1.29 mW for dmPFC-PAG terminal::ChR2, 2.84 ± 0.62 mW for dmPFC-aBLA terminal::eNpHR3.0, 9.72 ± 2.03 mW for dmPFC-aBLA terminal::ChR2, 3.00 ± 0.76 mW for aBLA::eNpHR3.0, 5.30 ± 1.26 mW for aBLA::ChR2, 8.40 ± 2.10 mW for dmPFC-DRN cell-body::ChR2, 4.40 ± 0.94 mW for

dmPFC-PAG cell-body::ChR2, and 10.50 ± 3.34 mW for dmPFC-aBLA cell-body::ChR2 mice (light intensity measured at fiber tips, mean ± SEM). The number of light on trials before rank change was 0 - 2 for dmPFC-DRN terminal::eNpHR3.0, 0 - 2 for dmPFC-DRN terminal::ChR2, 0 - 7 for dmPFC-PAG terminal::eNpHR3.0, 0 - 1 for dmPFC-PAG terminal::ChR2, 0 - 3 for dmPFC-aBLA terminal::eNpHR3.0, 0 - 5 for dmPFC-aBLA terminal::ChR2, 0 - 2 for aBLA::eNpHR3.0, 0 - 5 for aBLA::ChR2, 0 - 2 for dmPFC-DRN cell-body::ChR2, 0 - 1 for dmPFC-PAG cell-body::ChR2, and 0 - 3 for dmPFC-aBLA cell-body::ChR2 mice.

For the inhibition or activation of dmPFC-DRN, dmPFC-PAG and dmPFC-aBLA (Figures 2 and 3), the rank change is in comparison to mCherry control on day 0. For the inhibition of pathways without behavioral effects including dmPFC-MDT (Figure 2), dmPFC-dmCPu and dmPFC-NAc (Figure S2), we compare the rank change to the rank of previous day (day-1). Tube tests on the test day were videotaped by a camera set aside the tube for annotation, and the detailed behaviors of rank-changed trials were further compared between light-off (before optogenetic stimulation) and light-on (rank changed) conditions.

For chemogenetic inhibition of the aBLA and pBLA, mice with hM4D virus expressed in bilateral aBLA or pBLA were grouped into 4 for the tube test. Mice with stable ranks received i.p. injection of clozapine-N-oxide (CNO, dissolved in saline, 5 mg/kg), while the cagemates were injected with comparable volume of saline. Ranks of the test mice were measured with tube test at 0, 0.5, 1.5, 6, 24 and 48 h after CNO injection.

RTPP test

Mice were placed in a white open box (52 × 26 × 23 cm) consisting of two chambers. In the first 10-min test, mice were allowed to freely move between chambers to test the basal place preference. Then, during the subsequent 10-min test, a stimulation side was assigned. Laser stimulation (473 nm, 5 Hz, 10 ms pulse width, 10 mW) was delivered as soon as mice entered the stimulation side and terminated once mice crossed to the non-stimulation side. A video camera positioned above the chamber recorded each trial. Mouse locations and velocity were tracked and analyzed using Any-maze software (Stoelting). The time in the light stimulation chambers before and during stimulation were calculated using Any-maze software (Stoelting).

Fiber photometry recording in tube test

The fiber photometry recording was conducted as described previously.[46] Mice were trained individually for 4 days. On the first 2 days, mice were trained to go through a 30-cm tube for 10 trials per day. On the next 2 days, they were trained for 10 trials per day to go through an elongated 60-cm tube with two movable doors (15 cm to the entries), where they would wait for a delay period (gradually increased from 0 to 5 s over training trials) before the door opened. From day 5, tube tests were carried out between cagemates in the elongated 60-cm tube. Two mice were gently released at the ends of tube. They waited at the doors for 5 s and then walked to the middle of the tube to compete. The 5-s delay period before gate-lift allowed us to record for a clean baseline without disruption from human handling. Since our photometry experiment requires a 1-s baseline, in order to reduce the potential contamination of the baseline signals from other behavioral epochs (such as resistance, push-back etc.), we chose well-trained mice so that low-rank mice would retreat quickly after high-ranked opponents initiated pushes. Behaviors were videotaped and annotated using BORIS software.[95]

The calcium signals of both winner and loser mice were simultaneously recorded using the fiber photometry system (ThinkerTech, Nanjing). A beam of 488 nm excitation light was delivered and the GCaMP fluorescence signals were acquired at a sampling rate of 50 Hz. The laser intensity was adjusted to a low level (40 μW) at the tip of optic fiber to minimize bleaching. To synchronize the video and fiber photometry recording, we simultaneously captured the video and fiber photometry recording interface and calculated the time difference between the two. For the peri-event time histograms (PETHs) analysis, the onsets of each push behavior were aligned to time zero and the signals were standardized using Z score. Baseline activities were calculated from -1 s to 0 s before each behavioral epoch. Permutation test was applied to analyze the statistical significance of the fluorescence response, as previously reported,[46,97] by comparing the distribution of Z score at each time point to the baseline period. p values were further corrected for multiple comparisons using FDR. The normalized area under curve (AUC) was also calculated to detect the fluorescence changes during pushes.

Anterograde and retrograde tracing

For the anterograde tracing experiments, mice were perfused 4 weeks after the injection of AAV2/8-hSyn-Synaptophysin-mRuby-T2A-H2B-EGFP into the dmPFC. To quantify the synaptic density, the average fluorescent intensity in target downstream regions of the dmPFC was calculated using ImageJ (National Institutes of Health). Then, fluorescent intensity of unlabeled region (background) was subtracted. The normalized fluorescent intensity was calculated as the background-subtracted intensities of each brain region divided by the fluorescent intensity at the dmPFC injection site.

For the retrograde tracing experiments, we first verified that the CTB injections were localized within the target brain regions (aBLA, DRN and PAG). To confirm retrograde labeling of aBLA-projecting, DRN-projecting, and PAG-projecting neurons in the dmPFC, coronal sections containing the dmPFC were imaged with an Olympus VS120 virtual microscopy slide scanning system. For each subject, the number of CTB-labeled cells within the dmPFC and the distance from the midline of each CTB-labeled cell were measured using ImageJ (National Institutes of Health).

Please cite this article in press as: Xin et al., Deconstructing the neural circuit underlying social hierarchy in mice, Neuron (2024), https://doi.org/10.1016/j.neuron.2024.11.007

In vivo electrophysiological recording in head-fixed mice

Acute *in vivo* optrode recording was performed in mice with ChR2 or eNpHR3.0 expression in aBLA- or DRN- projecting neurons of the dmPFC, respectively. Before the day of recording, mouse was deeply anesthetized with isoflurane. A stainless-steel head-plate was cemented with dental acrylic and the silver wires with two screws were attached to the skull as ground. After a craniotomy (0.5-1.0 mm in diameter) was made over the dmPFC, the brain surface was covered by silicone elastomer (Kwik-Sil, WPI) for protection. Then, the anesthesia was stopped. After recovery from the anesthesia, mice were headfixed to stereotaxic apparatus for 2-h habituation. On the day of recording, the mouse was headfixed in the stereotaxic apparatus. The silicone elastomer and dura matter were removed immediately before the insertion of the optrode. The optrode consisted of a 16-channel electrode with a 105 μm core optic-fiber (A1 3 16-5 mm-25-177-OCM16LP, NeuroNexus) terminated at the top recording site. We applied 10-s blue light pulses (473 nm, 5 Hz, 10 ms pulse width, 10 mW at fiber tip, 30 repetitions) or 10-s constant yellow light (589 nm, constant, 5 mW at fiber tip, 30 repetitions) for activation or inhibition through the optic fiber while recording through the electrode. The thin dimension of the silicon electrode probe allowed us to specifically target layer 2/3 or layer 5 of the dmPFC. For the activation or inhibition of DRN-projecting neurons, we targeted the optic-fiber in layer 5 while recording in layer 2/3. Conversely, for the activation or inhibition of aBLA-projecting neurons, we targeted the optic-fiber in layer 2/3 while recording in layer 5. The optrode was gradually lowered from -1.2 mm to - 1.6 mm to record units at different *Z* axis locations, which were verified by DiI-labeled electrode track at the end of the experiment.

Wide band electronic signals (0.05-8000 Hz) were sampled at 40 kHz with gain of 5000 by the OmniPlex Neural Data Acquisition System (Plexon). Spontaneous spiking signals were band-pass filtered between 300 and 8000 Hz. Common median reference (CMR) was assigned as a digital reference. Spike waveforms were identified by threshold crossing and sorted into units (presumptive neurons) by principal component analysis (PCA) using the Offline Sorter (Plexon). We excluded spikes with inter-spike intervals (ISIs) less than the refractory period (1.4 ms). Cross-correlation histograms were plotted to ensure that no unit was discriminated more than once on each recording site. Neurons with a signal-to-noise ratio < 2 and baseline firing rate < 1 Hz were excluded from further analysis. A unit was classified as wide-spike neuron if its peak-trough distance was > 400 μs. To detect light-induced changes of each recorded neuron (activated, inhibited or no response), the *Z* score of the whole light-on epoch was compared to baseline period using a Wilcoxon signed-rank test. The mean firing rates of the light-off and light-on period were also compared to detect the light-induced changes of the whole neuronal population.

In vitro electrophysiological recording

Mice were anesthetized intraperitoneally with 1% sodium pentobarbital (100 mg/kg body weight) and then perfused with 20 ml ice-cold dissection buffer (220 mM sucrose, 2 mM KCl, 1.15 mM NaH_2PO_4, 0.2 mM $CaCl_2$, 26 mM $NaHCO_3$, 6 mM $MgCl_2$ and 10 mM glucose, oxygenated with 95% O_2 and 5% CO_2). Brains were quickly dissected out after decapitation. Coronal slices (300 μm in thickness) were sectioned using a vibratome (VT1200S, Leica) in oxygenated chilled dissection buffer. The slices were then incubated in aCSF (125 mM NaCl, 2.5 mM KCl, 25 mM $NaHCO_3$, 1.25 mM NaH_2PO_4, 25 mM glucose, 1 mM $MgCl_2$, 2 mM $CaCl_2$ and 1 mM sodium pyruvate, oxygenated with 95% O_2 and 5% CO_2) at 32 - 34°C to recover for 1 h and then transferred to room temperature. Cells were visualized with Olympus microscope (BX51W1) equipped with infrared differential interference contrast optics. A MultiClamp 700B amplifier controlled by DigiData 1550 digitizer and pCLAMP10 software was used for recording (Axon Instruments). Whole-cell recording was conducted using glass pipettes with a typical resistance of 4 - 6 MΩ.

To test the function of the expressed ChR2 protein in dmPFC terminals, we injected AAV2/9-CAG-hChR2 (H134R)-tdTomato into the dmPFC. The neurons of the aBLA were recorded when optogenetically stimulating dmPFC terminals within the aBLA. The internal solution containing 150 mM K-Gluconate, 5 mM NaCl, 1 mM $MgCl_2$, 2 mM Mg-ATP, 0.5 mM Na-GTP, 0.2 mM EGTA and 10 mM HEPES (pH was adjusted to 7.2-7.3 with KOH) was used. A series of light protocols (473 nm; 10 ms pulse width; 5 Hz, 10 Hz, 20 Hz and 50 Hz) were delivered through an optic fiber close to the recorded regions. Current-clamp recordings (I = 0 pA) were applied in the aBLA neurons to record the evoked action potentials under different light frequencies.

To verify how aBLA-projecting neurons affect DRN-projecting neurons in the dmPFC, we expressed ChR2 tagged with enhanced green fluorescent protein (EGFP) in aBLA-projecting neurons and visualized DRN-projecting neurons with red fluorescence as described above. Light pulses (473 nm, 5 ms pulse width) were delivered to stimulate the aBLA-projecting neurons. Voltage clamp recordings were conducted in DRN-projecting neurons using an internal solution containing 115 mM $CsMeSO_3$, 20 mM CsCl, 10 mM HEPES, 2.5 mM $MgCl_2$, 4 mM Na-ATP, 0.4 mM Na-GTP, 10 mM Na-phosphocreatine, 0.6 mM EGTA and 5 mM QX-314 (pH was adjusted to 7.2-7.3 with CsOH). Light-evoked excitatory and inhibitory postsynaptic currents (eEPSCs and eIPSCs) were measured at -60 mV and 0 mV holding potentials, respectively. Ten sweeps were taken and averaged at each potential. The peak amplitude and onset latency (10 % rise time) were calculated from the averaged trace for each cell using custom-written MATLAB program. To evaluate monosynaptic transmission from aBLA-projecting neurons to DRN-projecting neurons, tetrodotoxin (TTX, 1 μM) was perfused into recording solution. Afterwards, 4-aminopyridine (4AP, 1 mM) was further added and perfused into recording solution. To confirm the inhibitory currents evoked by light, $GABA_A$ receptor antagonist picrotoxin (PTX, 100 μM) were added during the recordings.

To verify which type of interneurons modulate the inhibition from layer 2/3 to layer 5 neurons in the dmPFC, we expressed eNpHR3.0 in PV or SST neurons, respectively, in the dmPFC. In the same mice, we also expressed ChR2 in aBLA-projecting dmPFC neurons. Yellow light pulse (589 nm, 45 ms) was triggered 20 ms before the onset of the blue light pulse (473 nm, 5 ms) to ensure that PV or SST neurons were sufficiently suppressed when aBLA-projecting neurons were stimulated. Voltage clamp recordings were

conducted in layer 5 neurons using an internal solution containing 115 mM $CsMeSO_3$, 20 mM CsCl, 10 mM HEPES, 2.5 mM $MgCl_2$, 4 mM Na-ATP, 0.4 mM Na-GTP, 10 mM Na-phosphocreatine, 0.6 mM EGTA and 5 mM QX-314 (pH was adjusted to 7.2-7.3 with CsOH). Blue light-evoked inhibitory postsynaptic currents (eIPSCs) were measured at 0 mV holding potentials. Ten sweeps were taken and averaged. The peak amplitude was calculated from the averaged trace for each cell using custom-written MATLAB program, and compared between yellow light off and on.

QUANTIFICATION AND STATISTICAL ANALYSIS

All data are presented as mean ± SEM unless otherwise specified. Statistical analyses were performed with Prism 7.0 (GraphPad Software) or MATLAB2021a (MathWorks). All statistical tests were two-tailed, and results were considered statistically significant when the *p* value was less than 0.05. Normality and equal variances between group samples were assessed using the D'Agostino and Pearson omnibus normality test and Brown-Forsythe tests, respectively. When normality and equal variance between sample groups were achieved, the paired t test, unpaired t test, one-way repeated-measures ANOVA or two-way repeated-measures ANOVA with multiple comparisons was used. When normality or equal variance of samples was not met, the Wilcoxon matched-pairs signed rank test, Mann-Whitney U test or Friedman test with Dunn's multiple comparisons was performed. More detailed statistical information is provided in Table S1.